University of Nevada, Reno

Impact of Potential Climate Change on Predicted Fluvial Transport of Mercury and Associated Bioaccumulation along the Carson River-Lahontan Reservoir System

A thesis submitted in partial fulfillment of the
requirements for the degree of Master of Science in
Hydrology

by

Allison Flickinger

Dr. Rosemary Carroll/Thesis Advisor

May, 2015

THE GRADUATE SCHOOL

We recommend that the thesis
prepared under our supervision by

ALLISON FLICKINGER

Entitled

Impact of Potential Climate Change on Predicted Fluvial Transport of Mercury and Associated Bioaccumulation along the Carson River-Lahontan Reservoir System

be accepted in partial fulfillment of the
requirements for the degree of

MASTER OF SCIENCE

Rosemary W.H. Carroll, Ph.D., Advisor

John J. Warwick, Ph.D., Committee Member

Rina Schumer, Ph.D., Graduate School Representative

David W. Zeh, Ph.D., Dean, Graduate School

May, 2015

ABSTRACT

Historic mining practices have left the Carson River and Lahontan Reservoir (CRLR) system contaminated with high levels of mercury (Hg). Hg levels in Lahontan Reservoir planktivorous and predatory fish exceed federal human consumption limits. Inputs of Hg to the system are a result of contaminated bank erosion during high flow and diffusion from contaminated bottom sediments during low flow. The United States Bureau of Reclamation has produced future streamflow estimates for 2000-2099 using 112 CMIP3 climate projections and the Variable Infiltration Capacity (VIC) model. VIC results suggest that the hydrology of the system is likely to experience increased frequency of both high and low extreme flows, and the monthly averages of future flows are expected to be higher in the winter and lower in the summer compared to historical simulated flows. The VIC streamflow projections and modeled reservoir outputs are prepared as input for a Hg transport model, which consists of three numeric codes dynamically coupled (RIVMOD, WASP5, and MERC4). The dissolved methylmercury (MeHg) simulated from these models runs are used as input for a bioenergetics and mercury mass balance model (BioHg) which computes the bioaccumulation of MeHg in Sacramento blackfish in the Lahontan Reservoir. Model results suggest that loads of total Hg, total MeHg, and dissolved MeHg will decrease most significantly in the spring and summer due to the channel width increases and the depth decreases which reduce bank erosion over the century. Dissolved Hg loads increase in both the winter and spring, but decrease in the summer. An increase in channel bottom area leads to a higher rate of diffusive flux of dissolved Hg. Bioaccumulation levels may increase in both the South and Middle

Basins of the reservoir as a result of an increase in dissolved MeHg concentrations, but decrease in the North Basin due to mercury settling out in the upstream sections of the reservoir and the dilution effect of the Truckee Canal input near the Lahontan Dam. All three sections of the reservoir will maintain fish Hg levels above the federal action limit for consumption.

ACKNOWLEDGEMENTS

I would not have been able to complete this study without the financial, technical, and personal support that I have received.

This project was supported by the Grant/Cooperative Agreement Number G11AP20092 from the United States Geological Survey (USGS) and also by the Desert Research Institute.

My thesis committee has been invaluable to me throughout the entire process. I am grateful to Dr. Carroll for her patience and her willingness to take on a student despite the distance, Dr. Warwick for his enthusiasm towards solving the bugs in the model even though it ended up being rather time consuming, and Dr. Schumer for her statistical insight and her edits which went a long way to improve this thesis.

I received technical support on several aspects of this project. I would like to thank Shane Coors for explaining the Lahontan Dam release operations, which allowed me to create the reservoir model. I am thankful to Matthew Sgambati for helping me get my jobs running on the grid and preventing me from submitting 112 jobs individually. Additionally, I greatly appreciate the computing resources that were available to me at both the Desert Research Institute and the University of Nevada, Reno.

And finally, I would like to thank my family, my boyfriend, and my friends. Without their encouragement and support this would have exponentially more difficult, if not impossible.

Table of Contents

LIST OF TABLES

LIST OF FIGURES

INTRODUCTION

Background:

In the United States, over 66,387 square kilometers of lakes and 1,841,161 kilometers of river were under advisory in 2011 due to elevated mercury (Hg) levels (EPA, 2013). The severity of the situation has led to the development and use of numerical models in order to understand and predict what happens in Hg contaminated waters (Somlyody 1978; Fontaine 1984; Petrie and Yeats, 1990; Martin 1992; Bale 2000). Numerical models can capture the complex processes associated with Hg cycling and transport that analytic approaches cannot.

The Hg cycle contains several forms of Hg, with transformations occurring in certain conditions. The elemental form of mercury, Hg^0, is highly volatile and has a relatively low solubility in water (Lindqvist and Rodhe, 1985). Inorganic mercury, Hg^{2+}, exists more readily in fresh water and can be dissolved or sorbed to particles in the water with a greater affinity for sorption to fine particles due to increased surface area (McCutcheon et al., 1992). Hg^{2+} is transformed into methylmercury (CH_3Hg^+, or MeHg) through the process of methylation. MeHg is produced primarily through methylation by sulfate reducing bacteria in anoxic sediments. Factors affecting the rate of methylation include temperature, pH and dissolved organic carbon availability (Miskimmin et al., 1992). The demethylation process can occur either as a result of bacteria, through oxidative or reductive demethylation, or as a result of light, through photodemethylation (Barkay and

Wagner-Dobler, 2005). Reductive demethylation produces Hg^0, oxidative demethylation produces Hg^{2+}, and photodemethylation produces both Hg^0 and Hg^{2+}.

MeHg is toxic to both humans and wildlife. It is a neurotoxin that negatively affects fetal development (Mergler et al., 2007). MeHg has a much higher biological uptake rate compared to inorganic Hg and is soluble in fat (Boudou and Ribeyre, 1997; Morel et al., 1998). An increase in MeHg concentration in an organism can occur over time if the organism ingests MeHg at a rate faster than it releases it. This increase in MeHg concentration in an organism over time is known as bioaccumulation. Biomagnification describes how MeHg concentration is higher in organisms in higher trophic levels due to predators eating food with high levels of MeHg.

We are interested in how a changing climate will affect the levels of Hg contamination in fluvial systems as well as human exposure to this toxic substance. Globally, climate change is expected to cause changes to the water cycle by increasing intense precipitation events and also increasing the length of the dry periods (Collins et al., 2013). Increased input of contaminants can occur during increased flows via enhanced erosion of contaminated riverbanks, and an increase in concentration of a contamination can occur during decreased flows due to reduced dilution (Whitehead et al., 2008; Schiedek et al., 2007). A decrease in flows can also increase residence times in lakes and reservoirs, which can lead to increased settling rates of sediments.

Projected climate and hydrologic data are necessary to model future changes in Hg transport models that require climatic or resultant boundary conditions. The World Climate Research Programme's Coupled Model Intercomparison Project phase 3

(CMIP3) has produced 112 climate projections that correspond with three different emissions scenarios (higher, middle, and lower path of emissions) to demonstrate possible climate changes during the next century (Meehl et al., 2007). The U.S. Bureau of Reclamation (USBR) down-scaled these climate projections for 195 sites throughout the Western US and used them as input to the Variable Infiltration Capacity model (VIC, Liang et al., 1994) to assess hydrologic responses to the climate projections (Gangopadhyay and Pruitt, 2011).

One of the rivers that the USBR has produced hydrologic projections for is the Carson River. The area around the Carson River was historically used for mining of silver and gold, and the river system is plagued by large amounts of contamination left behind in the environment. Total Hg levels (THg) have been observed from 645 to 2107 nanograms per liter (ng/L) in the river and 57 to 1582 ng/L in the Lahontan Reservoir, which is downstream of the river (Bonzongo et al., 1996). In comparison, the lake with the highest mean total Hg concentration in the Great Lakes region of the US was Lake Erie, with a concentration of 12 ng/L (Wiener et al., 2012). Total MeHg (TMeHg) levels are relatively low in the system considering the high levels of THg due to the alkalinity of the system, ranging from 1.8 to 7.2 ng/L in the river and 0.4 to 0.5 ng/L in the reservoir. Hg concentrations in the system vary depending on location, but upper bank materials that were deposited after mining began have been found to have an average Hg concentration of 99.9 micrograms per gram (μg/g) with a maximum concentration of 887 μg/g (Miller et al., 1998). These high levels of Hg in the water and soil led to the designation of the

Carson River as a Superfund site in 1991 by the United States Environmental Protection Agency (US EPA).

The purpose of this study is to use numeric models to assess how climate change will affect the transport and bioaccumulation of Hg in the Carson River and Lahontan Reservoir (CRLR) system.

Site Description:

The Carson River flows from the eastern Sierra Nevada Mountains into the Carson Playa. The river is primarily fed by snowmelt. In 1915, the Lahontan Reservoir was created behind the Lahontan Dam as part of the Newlands Irrigation Project. Besides providing water for agriculture, the reservoir also acts as a sediment trap and is managed as a warm water fishery. Figure 1 shows a map of the river and the reservoir, with the relevant sites marked with colored circles. All of the sites have USGS gage data available, but only the sites marked with red circles have USBR flow projections available.

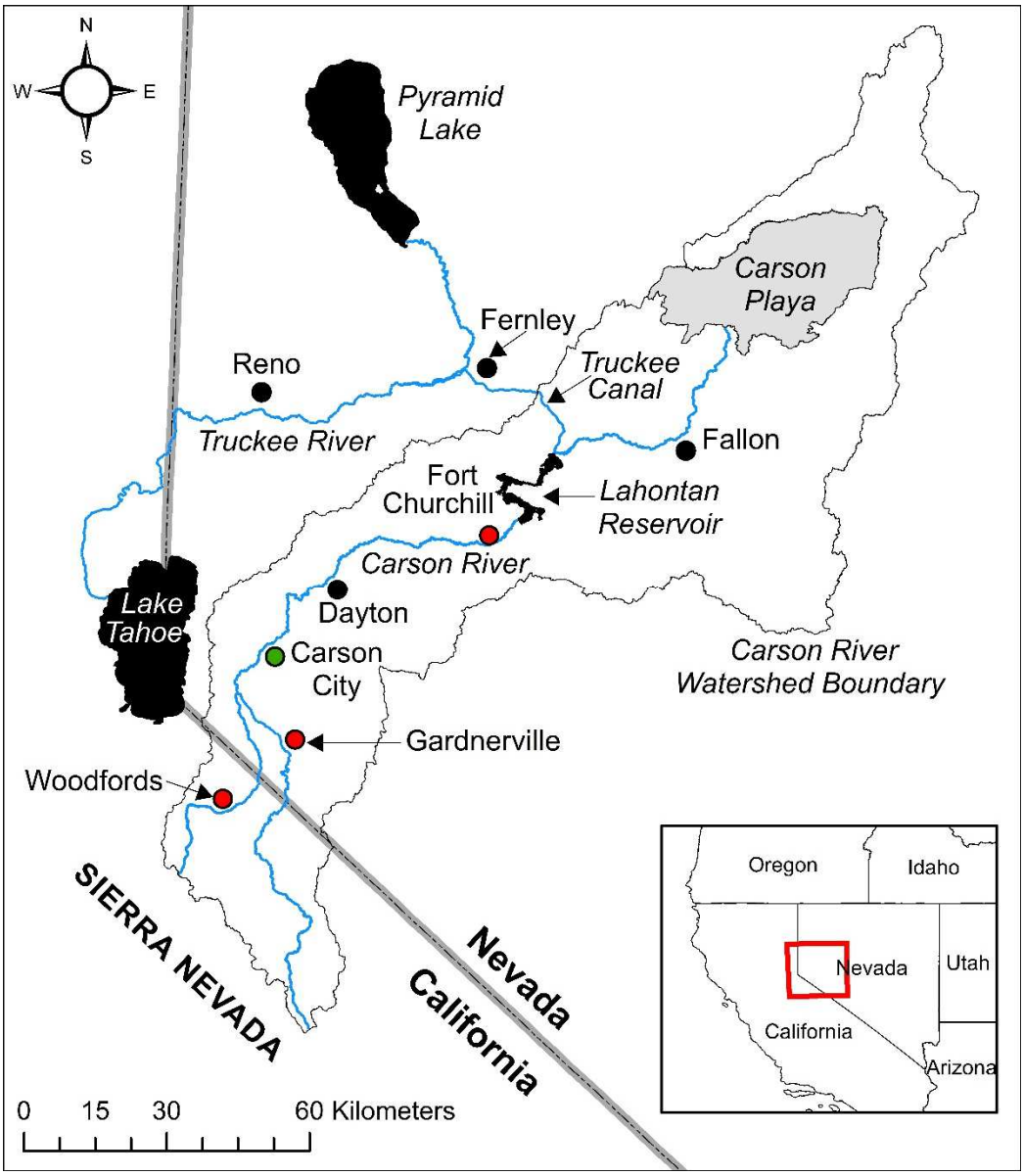

Figure 1: Map of Carson River with sites. The sites marked with a red circle indicate the sites with USBR flow projections available, and the site marked with the green circle, Carson City, is the site that is necessary as a boundary condition for the Hg transport model but lacks USBR flow projection data. Flow is from the Sierra Nevada Mountains northeast into Lahontan Reservoir and eventually to the Carson Playa.

At the height of the mining of the Comstock Lode in the 1860s and 1870s, it was estimated that the gold mines produced more than 5.44×10^5 kg of tailings, with varying amounts of Hg, daily (Smith and Tingley, 1998). It is believed that 6.36×10^6 kg of Hg

from these mine tailings remains stored in river bank sediments and floodplain deposits in the Carson River and Lahontan Reservoir (CRLR) area (Miller et al, 1998; Smith and Tingley, 1998). The Hg was deposited in river banks during the mining era due to channel aggradation and began to enter the CRLR system after the decline of mining as a result of downcutting and erosion. High flow events in the system can cause massive inputs of Hg through erosion, such as the rain-on-snow flood event in 1997 which released an estimated 1.81×10^8 kg of sediment and 1360 kg of Hg into the Carson River Lahontan Reservoir (CRLR) system (Hoffman and Taylor, 1998).

The elevated levels of Hg in the CRLR system are reflected by the bioaccumulation of MeHg in fish in the system. The Federal Action Limit for Hg in fish is 1 µg/g. Planktivorous species such as the Sacramento blackfish (*Orthodon microlepidotus*) exceed 1 µg/g, and the top predator in the Lahontan Reservoir, the Walleye (*Sander vitreus*), has been sampled with total body burdens near 7 µg/g and muscle tissue concentrations of 9µg/g (Cooper et al., 1983; 1985; E&E, 1998, Kris Urquhart, NDOW, phone conversation with Dr. Carroll, November, 2009). Because the fish in the CRLR system exceed the Federal Action Limit level, the Nevada State Health Division declared a no consumption advisory for the general public for all fish in the Carson River from Dayton to the Lahontan Dam and Lahontan Reservoir in 2007. Hg transport and bioaccumulation in the CRLR system are non-linearly related to streamflow (Carroll et al., 2000; Carroll et al., 2001; Carroll et al., 2004; Warwick and Carroll, 2008; Carroll, 2010). This means the magnitude of change on the Hg transport and bioaccumulation in the system may not be proportional to the change in hydrology due to climate change.

In the next century, Nevada is expected to experience temperature increases of 3-4 degrees Celsius in the spring and fall and 5-6 degrees Celsius in the winter and summer (CIER, 2008). The summers are expected to become more arid, and the winters are expected to become more wet, with a shift from mountain snow to rain. Along with increased winter runoff, this will also cause a decrease in the snow pack and earlier melt out dates (Collins et al., 2013).

The USBR hydrologic simulations for sites along the Carson River reflect these predictions. For example, 2000-2099 flow projections for monthly average flows for the Fort Churchill site on the Carson River are generally higher in the winter and lower in the spring than the VIC simulated flows during the historical period, 1950-1999 (Figure 2).

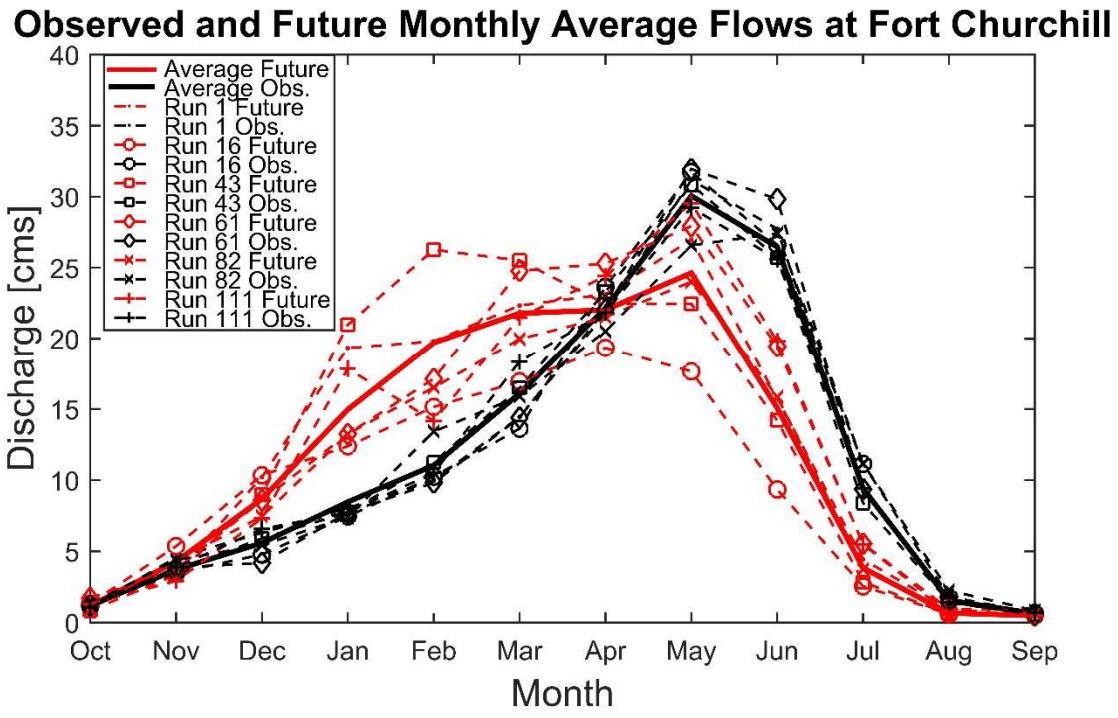

Figure 2: The monthly average flows of the projections in the historical period (black) and future period (red) at Fort Churchill are shown for several of the climate projections, and also for the average of all 112 climate projections.

Future projected daily flows have a higher frequency of extreme lows and extreme highs than the projected flows in the historical period (Figure 3 and Figure 4). Low flows were defined as under 3 cubic meters per second (cms), and the extreme high flows were defined as at or above the overbank flow (110 cms) for the system. High flows were measured during 0.3778% of the historical period measurements while high flows occur in the future projections between 0.068 and 3.56% of the time with a median of 0.64 %. Low flows were measured during 36.8% of the historical period measurements, while low flows occur in the future projections between 33.26 and 50.26% of the time with a median of 42.35%.

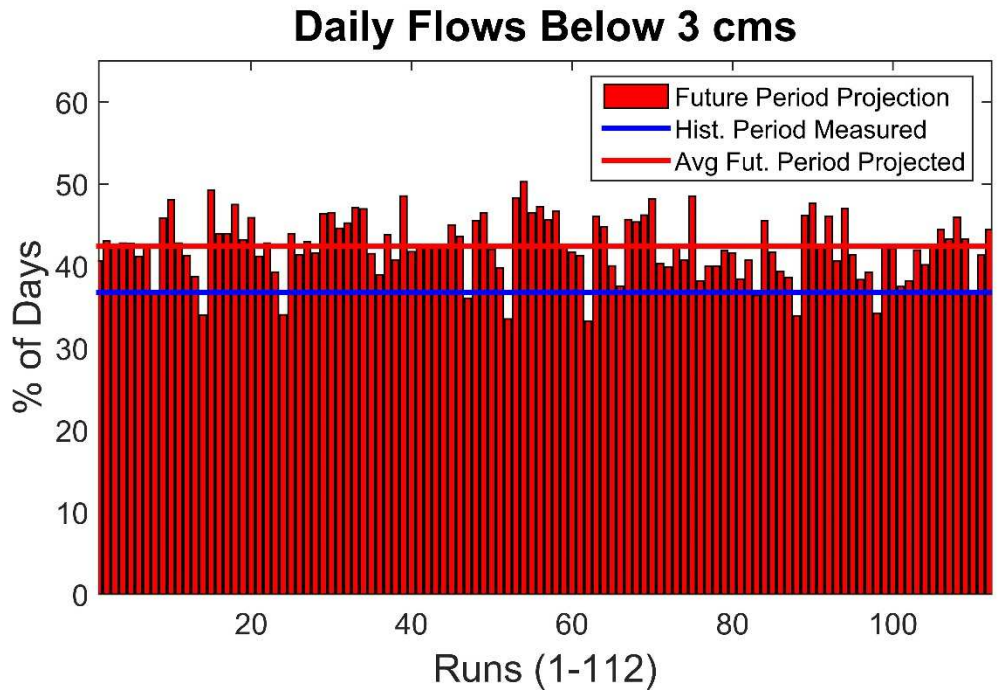

Figure 3: Percent of daily flows at Fort Churchill that are 0 cfs, shown by run number (1-112).

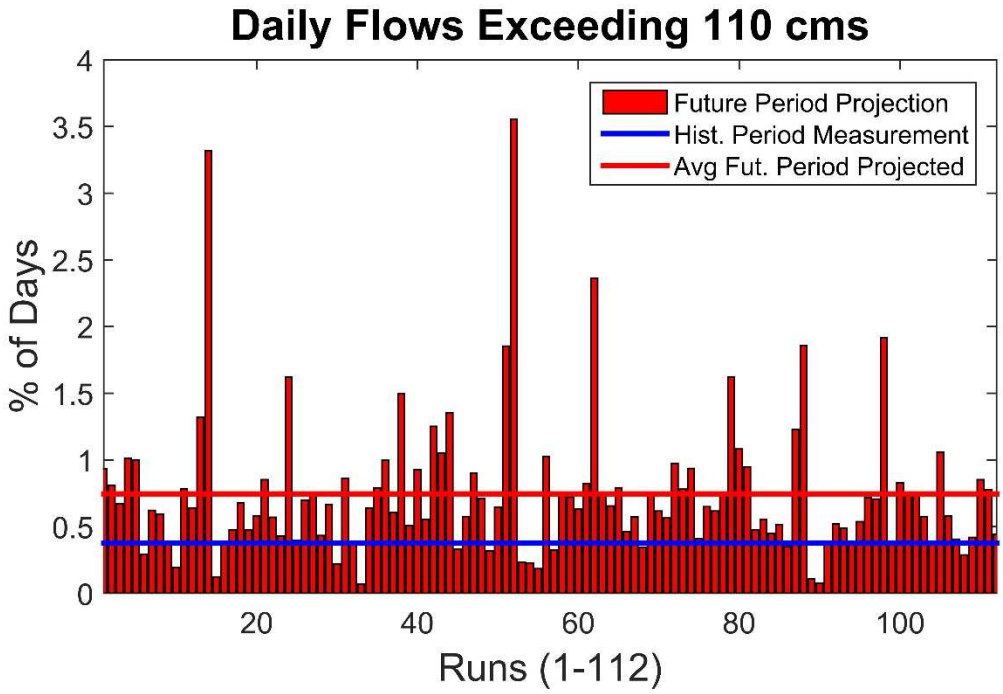

Figure 4: Percent of daily flows at Fort Churchill that exceed 110 cms, shown by run number (1-112).

Related Work:

Watershed models focusing on how Hg concentrations and cycling are affected by climate change have been developed and used for a coastal watershed where Hg from atmospheric deposition entering the aquatic system through watershed runoff was the main Hg input to the system (Golden et al., 2013). While atmospheric deposition is an important source of Hg for most aquatic systems and has been estimated to be responsible for 90% of the Hg loading of surface water (Wang et al., 2004; Leopold, 2010), the Hg entering the CRLR system through dynamic loading from bank and channel sediments is far greater than that of atmospheric deposition, and so a model that better accounts for this type of input is necessary to accurately model the CRLR system.

Many modelling studies have focused on the behavior of Hg in the CRLR system. Three programs developed by the US EPA, RIVMOD (Hosseinipour and Martin, 1990), WASP5 (Ambrose et al., 1991), and MERC4 (Martin, 1992), have been linked to investigate Hg in the CRLR system. RIVMOD is a hydrodynamic model that calculates velocities and depth by solving standard fluid equations of continuity (Equation 1) and momentum (Equation 2). The continuity equation was modified from the original RIVMOD version to account for changes in channel width (Equation 1; Warwick and Heim, 1995).

$$\frac{\delta Q}{\delta x} + \frac{\delta (B * y)}{\delta t} = q \qquad 1$$

$$\frac{\delta Q}{\delta t} + \frac{\delta}{\delta x}\left(\frac{Q^2}{A}\right) + qv = A\left(gS_0 - gS_f - g\frac{\delta y}{\delta x}\right) \quad 2$$

Where Q is the fluid flow (m^3/s), t is the time (sec), x is the distance (m), q is the lateral inflow to channels between stations (m^3/s), A is the channel cross sectional area (m^2), v is the velocity (m/s), S_0 is the channel bottom slope, S_f is the friction slope, y is the water depth (m), and B is the channel width (m).

The RIVMOD code has also been modified in order to model overbank flows more accurately. A divided channel approach was adopted that considers the floodplain separate from the main channel to estimate floodplain velocities and depths (Carroll et al., 2004).

WASP5 is a routine that simulates the transport and transformation of a variety of constituents by using mass balance equations to account for processes such as direct and diffuse loading, advective and dispersive transport, and physical/chemical transformation. WASP5's sediment transport has been improved to include simulation of three types of sediment: washload, coarse suspended sediment, and bedload.

MERC4 is a subroutine for WASP5 that computes Hg speciation and transformation. Hg species represented in the model include both the dissolved and sorbed inorganic Hg and MeHg. Elemental Hg only exists at low levels in the Carson River surface water (Bonzongo et al., 1996), and estimates for loss of THg to elemental Hg are low in the Lahontan Reservoir compared to other temperate systems because a high percent of THg occurs in particulate form, which limits the availability of THg to be volatilized (Gandhi et al., 2007). As a result, elemental Hg is not included in this study.

The CRLR model covers 112 km from Carson City to the Lahontan Dam in 307 segments, with channel geometry and floodplain characteristics specified for each segment. The calculation of Hg transport and flux is specified under four flow regimes: low, medium, high, and overbank (Carroll and Warwick, in review). The low flows, less than 3 cms, only account for diffusion from the bottom channel sediments (Equation 3):

$$\frac{\partial M^d}{\partial t} = \frac{EA\eta}{\epsilon/\eta}\left(\frac{C_b^d}{\eta} - C_w^d\right) \quad 3$$

Where M^d is the dissolved mass (mg) in the water column, t is time (s), A is interfacial area between the channel bottom and overlying water column (m^2), η is porosity, C_b^d and C_w^d are the dissolved chemical concentrations the channel bed sediments and overlying water column, respectively (mg/L), ϵ is the characteristic mixing distance (m) between the bed and the water column, E is the diffusion coefficient (m^2/s).

During medium flows, between 3 and 10 cms, diffusion from the channel bottom sediments is combined with turbulent mixing and advective transport (Equation 4 and 5):

$$\frac{\delta M^S}{\delta t} = B_f[v - v_C]AC_b^T(1 - f_b) \quad 4$$

$$\frac{\delta M^d}{\delta t} = B_f[v - v_C]AC_b^T(f_b) \quad 5$$

Where M^S and M^d are the sediment and dissolved components, or more precisely the fraction < 45 μm, of THg^{2+}, respectively, leaving the channel bed and entering the overlying water column, C_b^T is the concentration of THg^{2+} in the river channel bottom sediments, v is the modeled flow velocity of the water column segment (m/s), B_f is a suspension velocity factor (dimensionless), and f_b (dimensionless) is the fraction of

sediment pore water THg^{2+} that is either dissolved or affiliated with colloidal material that is available for advective flux out of the channel bottom and into the water column.

The Hg inputs during high flows, between 10 and 110 cms, are dominated by bank erosion, through which sediment bound and dissolved Hg enters the water column (Equation 6):

$$MER = \frac{\psi_1 \rho_s \gamma_w n^2 D^{2/3} v^2 L_s}{S_0^{1/2}} \quad 6$$

Where *MER* = total bank mass eroded, γ_w is the specific weight of water ($kg/m^2/s^2$), *h* is the height of the vertical bank face along the river's edge (m), *D* is the water depth starting at the vertical face of the channel bank (m), S_0 is the channel bottom slope, *v* is the water velocity (m/s), *n* is Manning's coefficient, L_S is the segment length (m) in the downstream direction, and ψ_1 is a constant of proportionality ($m^2 \cdot s/kg$).

Overbank flows occur when flow exceeds 110 cms, leading to bank erosion and overbank deposition on the floodplain. This is modeled (Equation 7) using a modified version of equation 6:

$$MER = \frac{\psi_1 \rho_s \gamma_w n^2 D^{2/3} v^2 L_s}{S_0^{1/2}} + \frac{\psi_2 \rho_s \gamma_w n^2 (D-h) v^2 L_s}{h^{1/3} S_0^{1/2}} \quad 7$$

Where an additional term, ψ_2, has been calibrated (Carroll et al., 2004) using observed total mass eroded from February 1991 through February 1997 (Miller et al., 1999).

Mercury levels within the Lahontan Reservoir have also been studied. Seasonal variation of Hg concentrations in the Reservoir is explained mostly by the Carson River Hg

loading, which doubles between spring and late summer (Carroll et al., 2011). MeHg partitioning in phytoplankton was found to be a function of Hg concentrations, reservoir residence time, and algal growth. Higher concentrations of MeHg were found in smaller particulate matter, which is associated with living biomass, during late summer.

The combination of mass balance and bioenergetics models is a commonly used and accepted technique in studies concerning bioaccumulation of Hg in fish (Trudel and Rasmussen, 2001). A bioenergetics and mercury mass balance model (BioHg) was created in order to model the body burdens in the Sacramento blackfish (Carroll, 2010). This model was calibrated using observations from Sacramento blackfish in the Lahontan Reservoir.

The BioHg uses dissolved MeHg data for the reservoir from the Hg transport model. There are two main parts of this model: bioenergetics and Hg mass balance. The first equation (Equation 8) is the bioenergetics equation which calculates the change in weight of the fish over time.

$$\frac{dW}{dt} = [C - (R + SDA + EG + EX)]\frac{ED_{prey}}{ED_{food}} * W - EGG * W \qquad 8$$

where C is consumption (g prey/g fish/day), R is respiration (g prey/g fish/day), SDA is specific dynamic action or losses due to digestion (g prey/g fish/day), EX is excretion (g prey/g fish/day), EG is egestation or losses due to feces (g prey/g fish/day), ED is energy density (J/g prey), W is weight (g), and EGG is the fraction of body weight lost to spawning (dimensionless).

The second equation (Equation 9) calculates the change in MeHg body burden over time.

$$\frac{dB}{dt} = (\alpha * C_{\delta} * I * W) - (E + K) * B \quad (9)$$

where α is assimilation efficiency of MeHg from food (dimensionless), C_{δ} is the MeHg concentration in the food (µg/g), I is the ingestion rate of fish (per day),W is weight (g), E is the elimination of MeHg (per day), K is the loss of MeHg to the gonads (per day), and B is the MeHg body burden (µg).

Modeling suggests that the difference between dynamic and constant loading of Hg does not cause a significant change in the computed body burdens in the Sacramento blackfish. This is a result of the uncertainty in dissolved MeHg water column concentrations. The dynamic loading of Hg, however, is useful for exploring how the decoupling of peak Hg loads and peak phytoplankton growth has the potential to affect the MeHg body burdens. If the timing of the peak Hg loads changes so that Hg concentrations in the reservoir are lower in the summer and higher in winter, this should decrease the Hg bioaccumulation rates in fish because their consumption rates peak in summer, and the Hg concentrations in their food will be lower.

MERCURY TRANSPORT MODEL

Data Preparation:

The Hg transport model requires the flow at the Carson City gage as a boundary condition, but the USBR does not have flow projections from the VIC model for this site. USGS measured discharges from Gardnerville, Woodfords were regressed against the Carson City gage to relate upstream and downstream flows in the Carson River and project flows at the Carson City gage. A linear regression in the log-log scale was performed for every month, comparing the combined Gardnerville and Woodfords daily flows to the Carson City daily flows. Regressions for the first and second halves of September and October were performed to increase their R-squared values, as they were the lowest of the months. Halving these months increased the R-squared values, suggesting that flows in these months are more varied than other months. Changing flow characteristics during these months could be due to the decrease in water use for irrigation around this time.

Application of the regressions to the combined upstream flows resulted in a set of modeled Carson City discharges, shown in Figure 5 for the period of 2000-2013. A comparison of the modeled and measured daily flows shows a satisfactory normalized root mean squared error (NRMSE) of 1.69 %. These regressions were then applied to the upstream boundary conditions at the Carson City Gage for hydrologic projections spanning 2000-2099.

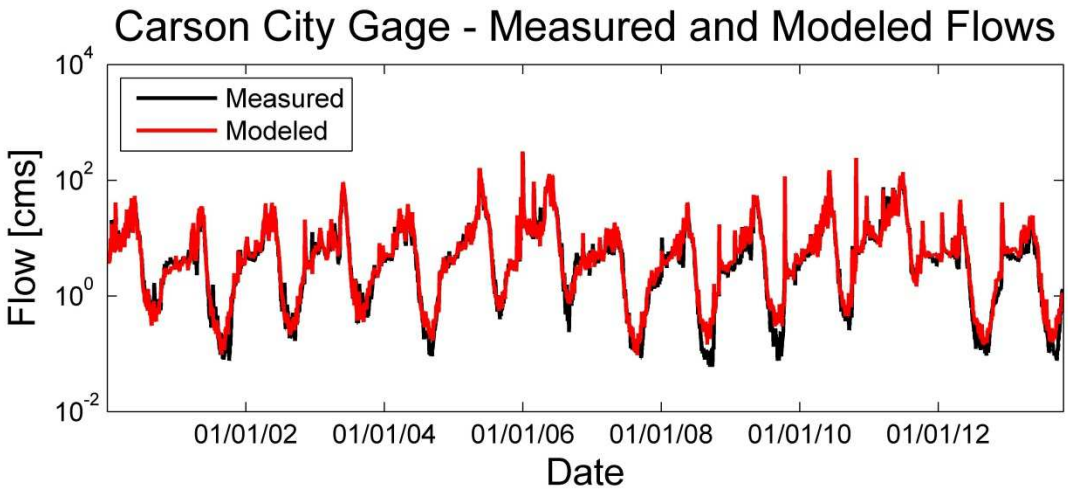

Figure 5: Hydrograph of Carson City flows from 2000-2013 showing the measured flows and modeled results based on regressions from VIC output for Gardnerville and Woodfords gages

The Hg transport model also requires flows at Fort Churchill in order to account for flow diversions upstream of the site. A comparison of USBR projected flows at Fort Churchill from 1950-1999 to the measured flows shows a high level of bias, so the bias-correction method from "West-Wide Climate Risk Assessments: Bias-Corrected and Spatially Downscaled Surface Water Projections" was used to bias-correct the projections (Gangopadhyay and Pruitt, 2011). Empirical cumulative distribution functions (ECDFs) of both the measured and the projected data from 1950-1999 were calculated. The modeled data were corrected by finding the percentile of the flow according to the ECDF of the modeled data, and then using the flow of the corresponding percentile from the ECDF of measured data as the bias corrected flow. Thus, original model ECDFs (Figure 6) were transformed so that the ECDF of the historical period projected data lines up with the ECDF of measured data (Figure 7). While the ECDF of the future period projected data is more similar to the ECDF of the measured data, it is still slightly different,

representing the increase in frequency of extreme flows in the future projected flows projected hydrologic changes (Figure 3 and Figure 4).

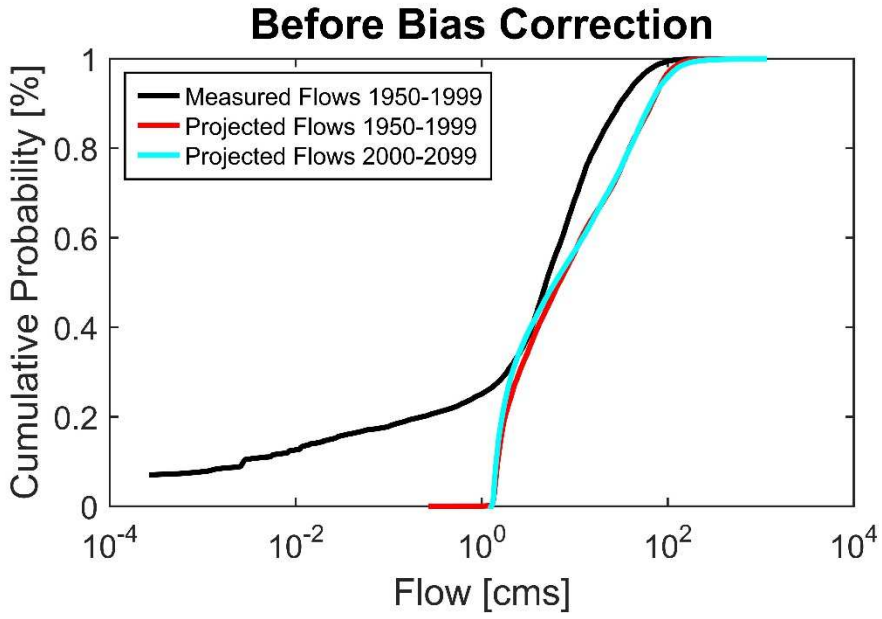

Figure 6: ECDFs of the measured flows and the projected flows of both the historical and future periods before bias correction

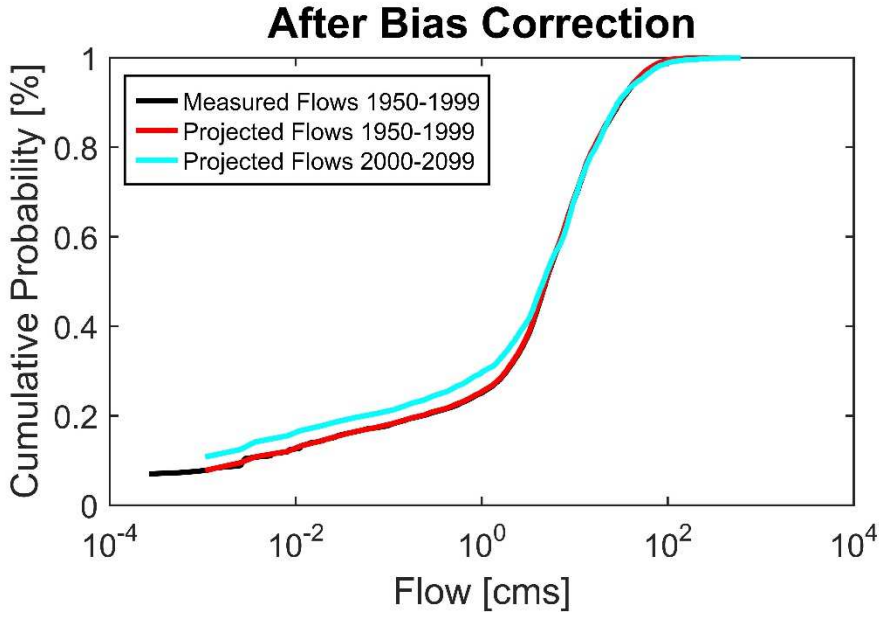

Figure 7: ECDFs of the measured flows and the projected flows of both the historical and future periods after bias correction

The Hg transport model also requires the daily discharge from the Lahontan Dam as a downstream boundary condition. A spread sheet model was developed to predict this variable. The model uses the projected Fort Churchill flows along with an averaged Truckee Canal as input. The discharge from the dam was determined by operational release rules that ensure enough water is available for agriculture by requiring a minimum amount of water to be discharged each year. The current annual demand for agriculture is approximately 339,207,000 m^3, and this is released at a constant daily flow from halfway through March to halfway through November (simplified to March through November for the model). The model follows the operational release rules which specify the proportion of this release for each month of the March to November growing season. Discharge from the dam was also determined by the maximum reservoir storage, as water must be released to prevent over topping at the dam.

The resulting predicted reservoir stage and discharge from the spread sheet model are shown in Figure 8 and Figure 9. The model was found to have an NRMSE of 12.63% for the reservoir stage and an NRMSE of 16.90% for the dam discharges. This error is in part due to the use of an average value for the monthly inputs from the Truckee Canal. The Truckee Canal flow is strictly regulated and the variations in flow do not directly line up with any other variable (such as the Carson River flow or Lahontan Reservoir storage) due to the other considerations in appropriating the Truckee River flow. The Truckee Canal can have a large impact on stage and storage of the reservoir under dry years, and so differences in the measured and average Truckee Canal inputs can create large errors during these periods. The impact of the Truckee Canal should be considered when

modeling Hg and bioaccumulation in the reservoir as it can dilute the concentrations of DMeHg in the northern section of the reservoir and over predict flow out of the dam during certain years.

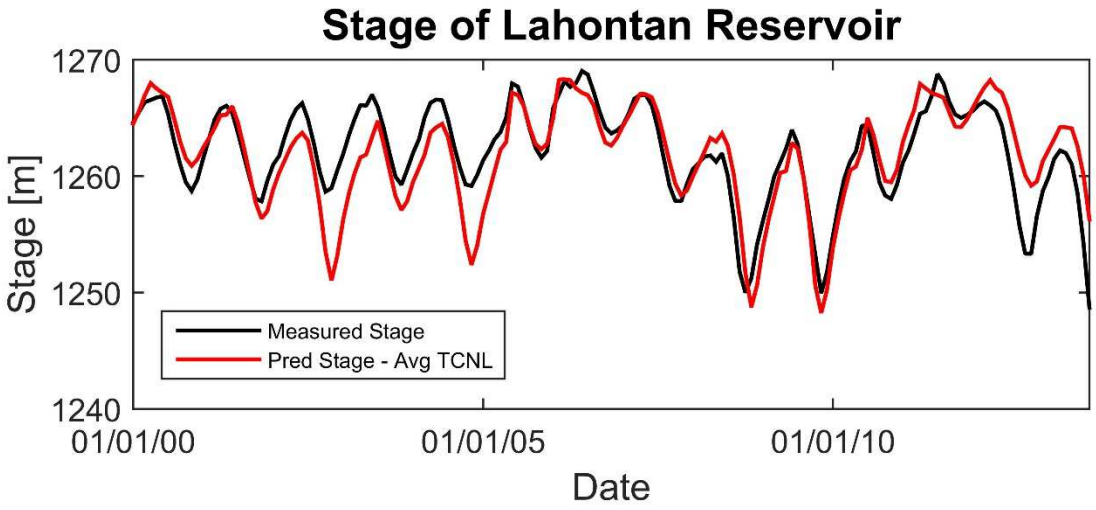

Figure 8: The stage results from the stage-storage spreadsheet, showing the measured stage and the stage predicted using the release rules and the averaged Truckee Canal flows

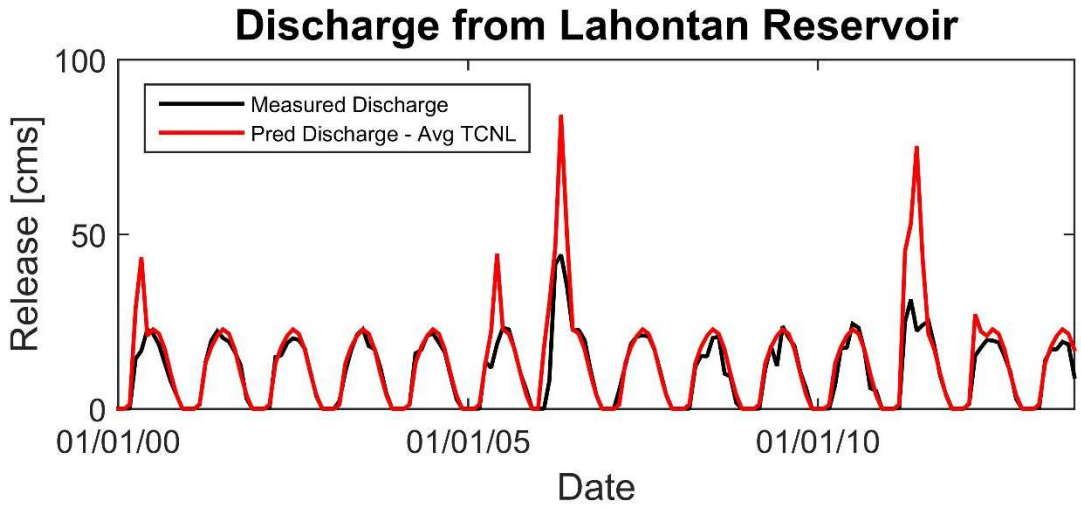

Figure 9: The Lahontan Dam discharge results from the stage-storage spreadsheet, showing the measured discharge and the discharge predicted using the release rules and averaged Truckee Canal flows

Model Modifications:

Several modifications were made to the Hg Transport model in order to ensure that the runs could accurately run for a century. The original model had not been run for longer than a decade, and early attempts to continue the model past a decade found that the time variables needed to have more significant digits in order to prevent round off error. There was also a numerical instability that was solved by limiting the maximum change in Hg concentration between time steps, and the accuracy of the results was improved by raising the maximum number of iterations per time step from 10 to 20.

Results Analysis:

The input files for each of the 112 runs of the model, representing the hydrologic projections for each of the 112 climate projections, were built and then run using the Hg transport model on both the DRI and UNR grid. Output for each Hg species and the total mass transported was analyzed for Fort Churchill and in each of the three basins of the reservoir (South Basin, Middle Basin, and North Basin – as shown in Figure 10). Each decade of results was averaged, and a range of values was found using the ranked 10^{th} and 90^{th} percentiles to determine an envelope around the averages. These ten decadal averages were then compared in order to determine if the change between them is significant.

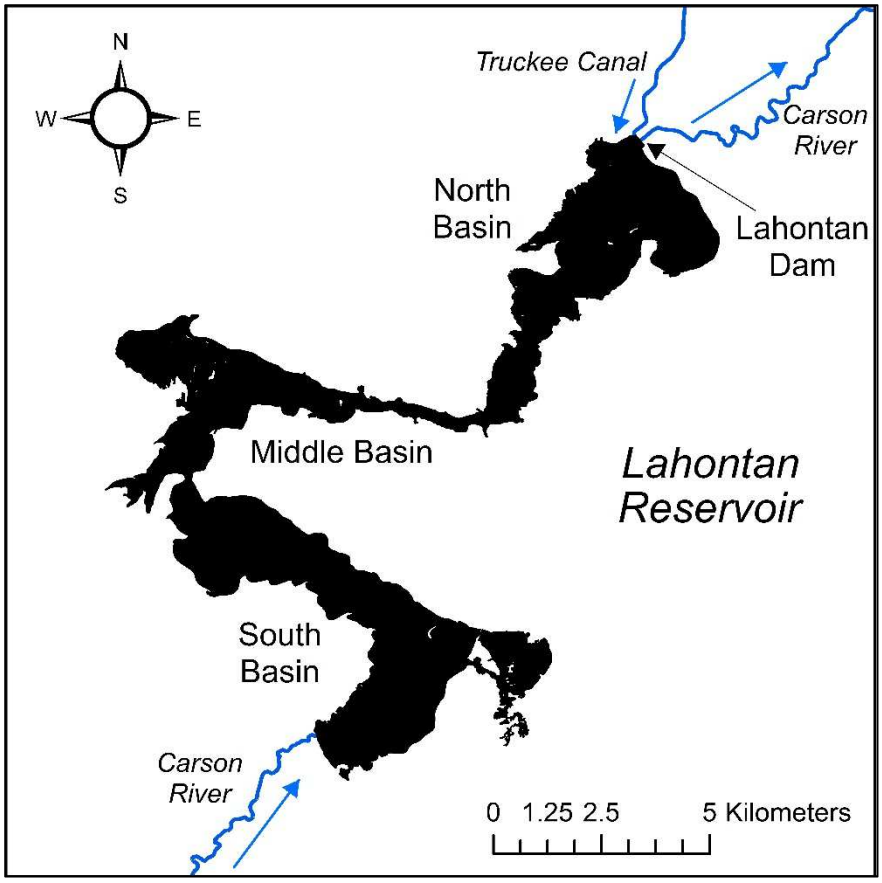

Figure 10: Map of the Lahontan Reservoir showing the South, Middle, and North Basin along with the Fort Churchill site.

The two-sample Kolmogorov-Smirnov test (K-S test) was used to determine whether the distribution of the Hg species results differs between each decade and the baseline decade (2000-2009) distribution. This test determines significance using the largest difference between two empirical distribution functions, as shown in Figure 11. The two samples are determined to be significantly different if the following equation (Equation 10) is true:

$$D_{n,n'} > c(\alpha)\sqrt{\frac{n+n'}{nn'}} \qquad 10$$

Where $D_{n,n'}$ is the largest difference between the two empirical distribution functions, $c(\alpha)$ is the coefficient of α, the significance level (1.36 for a significance level of 5%), and *n* and *n'* are the sizes of the two samples being compared.

This test has been used in other studies to compare flow outputs from different models and emissions scenarios (Risley et al., 2011; Maurer et al., 2010; Miller et al., 2010).

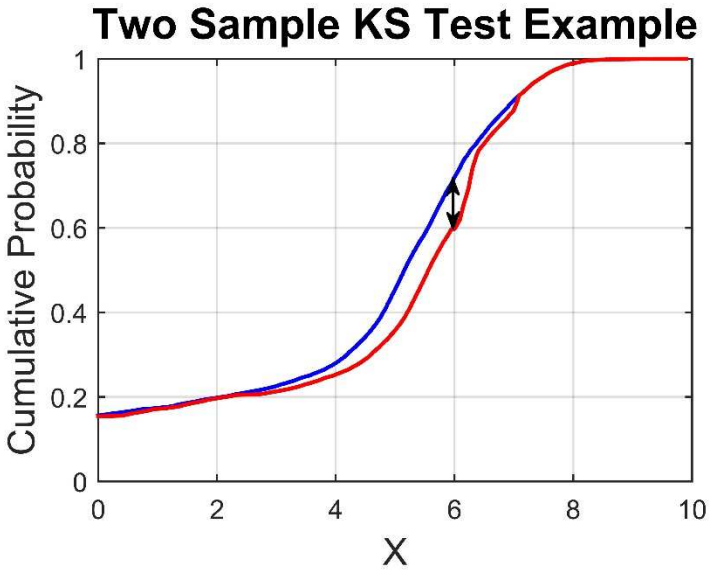

Figure 11: Example showing how the two sample KS test works

The K-S test was used to look at the Hg distributions by season in addition to decade, as the distribution of the Hg species is seasonally dependent due to the difference in flow regimes during these seasons and the variation in Hg loading mechanisms between the flow regimes.

Mercury Transport Model Results:

Weeks Bridge was the location used to analyze the changes happening in the river, as this has been a location that samples have been taken in the past. It is also just upstream of the river delta into the Lahontan Reservoir, making it a surrogate for Hg loading into the reservoir. The depth in the first decade has a strong peak around May/June (Figure 12), but over the decades the peak becomes less distinct and shifts earlier in the year to spring. The depth decreases overall by the end of the century. The flow at Weeks Bridge also peaks around May/June in the first decade, while the last decade has higher flows in the winter/spring and lower flows in the summer (Figure 13).

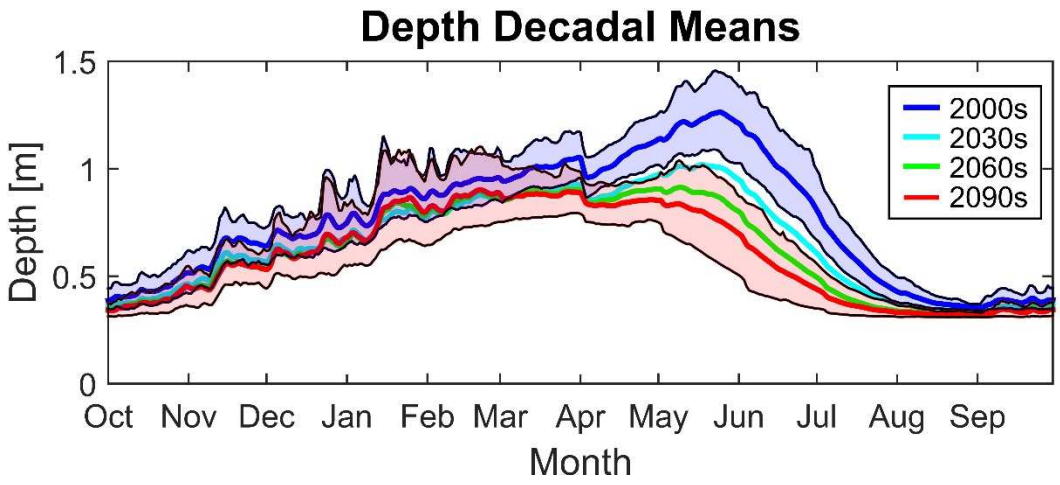

Figure 12: Decadal means of channel depth at Weeks Bridge, with the first and last decades enveloped by the 10th and 90th percentiles.

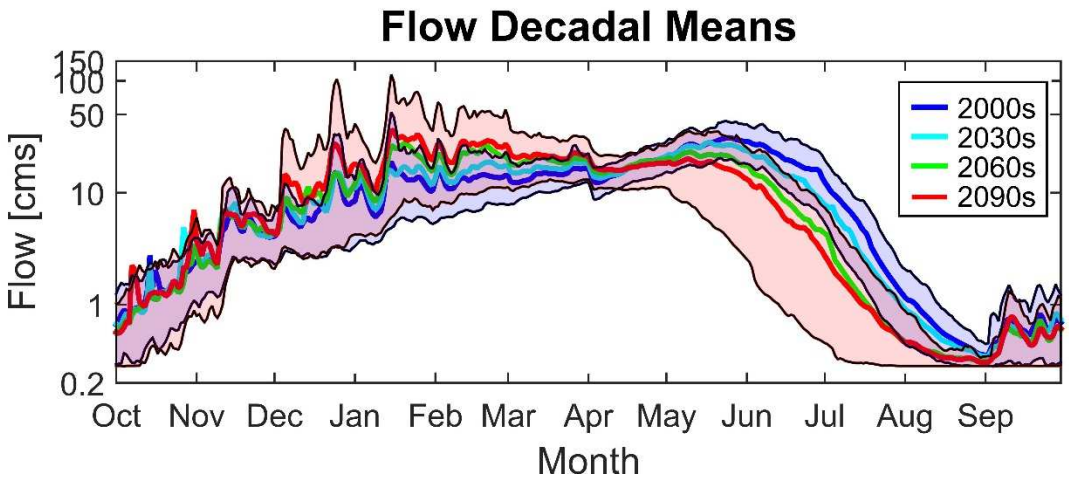

Figure 13: Decadal means of streamflow at Weeks Bridge, with the first and last decades enveloped by the 10th and 90th percentiles.

The change in flows in terms of the four flow regimes of the Hg transport model is seen in Table 1. There is an increase in high flows in the winter, with a decrease in medium flows and over twice the frequency of overbank flows. Spring shows an increase in low flows and a decrease in high flows. A large increase in low flows occurred in the summer of the last decade, along with a decrease in medium and high flows. Fall did not have as large of change as the other seasons, with only a slight decrease in medium flows.

Table 1: The percentage of days within the different flow regimes for the first and last decade of the century (averaged for all runs).

	% of Days Within Flow Regime	
Flow Regime	First Decade	Last Decade
	Winter (DJF)	
Low	25.38	24.05
Medium	52.69	42.30
High	20.89	30.85
Overbank	1.04	2.79
	Spring (MAM)	
Low	1.74	5.36
Medium	26.15	29.41
High	71.43	64.16
Overbank	0.68	1.07
	Summer (JJA)	
Low	49.97	74.51
Medium	24.20	17.14
High	25.65	8.28
Overbank	0.18	0.08
	Fall (SON)	
Low	78.14	79.98
Medium	19.24	16.83
High	2.55	3.08
Overbank	0.07	0.11

Concentrations of total inorganic Hg (THg) decrease overall throughout the century, and the peak that can be seen in the first decade around May and June is nonexistent by the last decade (Figure 14). While concentrations of dissolved inorganic Hg (DHg) increase over the century, the temporal variation of the concentrations remains similar throughout the century (Figure 15).

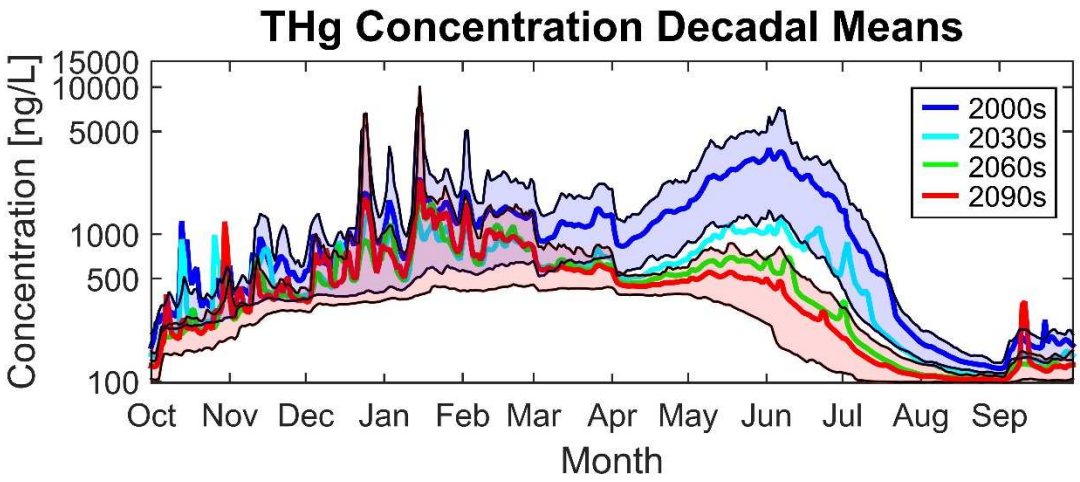

Figure 14: Decadal means of total inorganic Hg at Weeks Bridge, with the first and last decade enveloped by the 10th and 90th percentiles.

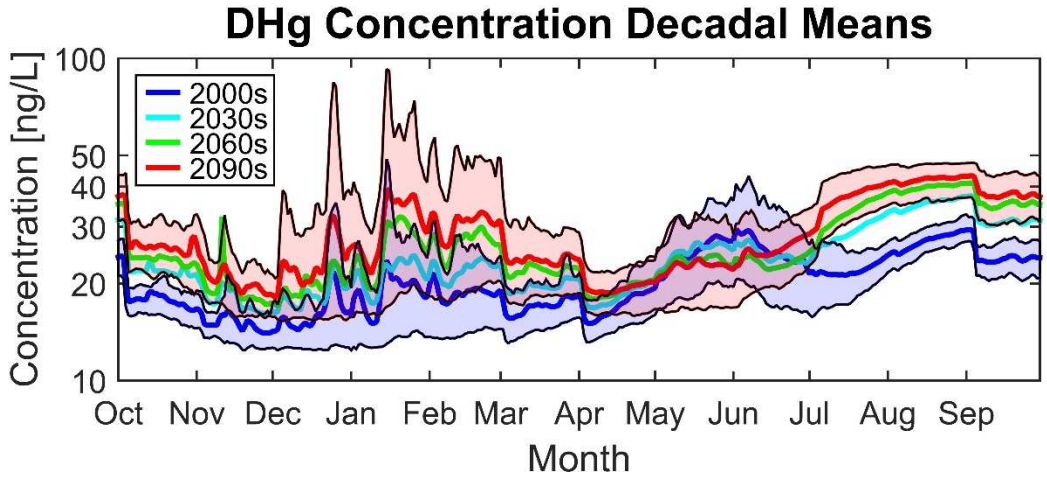

Figure 15: Decadal means of dissolved inorganic Hg at Weeks Bridge, with the first and last decade enveloped by the 10th and 90th percentiles.

The concentrations of the total methylmercury (TMeHg) decrease over the century, with the temporal variation of the concentrations remaining similar (Figure 16). The change in dissolved methylmercury (DMeHg) differs by season. The concentrations of DMeHg are lower in the winter by the end of the century but higher in the late spring/early summer, (Figure 19).

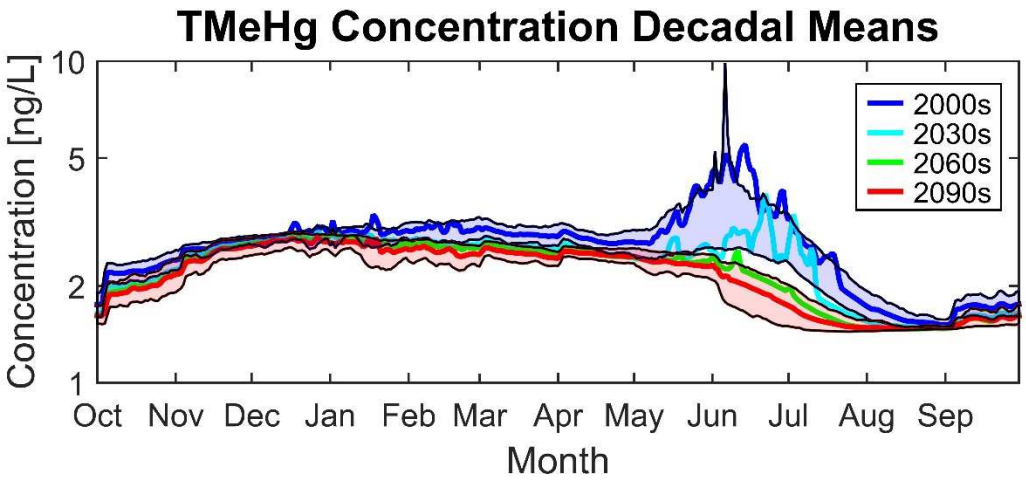

Figure 16: Decadal means of total methylmercury at Weeks Bridge. The first and last decade are enveloped by the 10th and 90th percentiles.

The decadal means of TMeHg concentrations (Figure 16) show the mean concentration exceeding the 90th percentile in June in the first decade. This occurs in the graphs for the loading rates of the Hg species as well. A further investigation of this showed that this is a result of high concentrations that are extreme outliers skewing the mean. The quantity of the outliers can be seen in the boxplot of the 112 decadal means taken for a day in the year where the mean exceeded the 90th percentile (Figure 17). A cumulative distribution function represents for each value the percentage of data that has a lower value. The shape of the empirical cumulative distribution function of the same data shows that the outliers cause the right side of the function to extend far beyond the curve in the function because their values are much higher than the majority of the data (Figure 18).

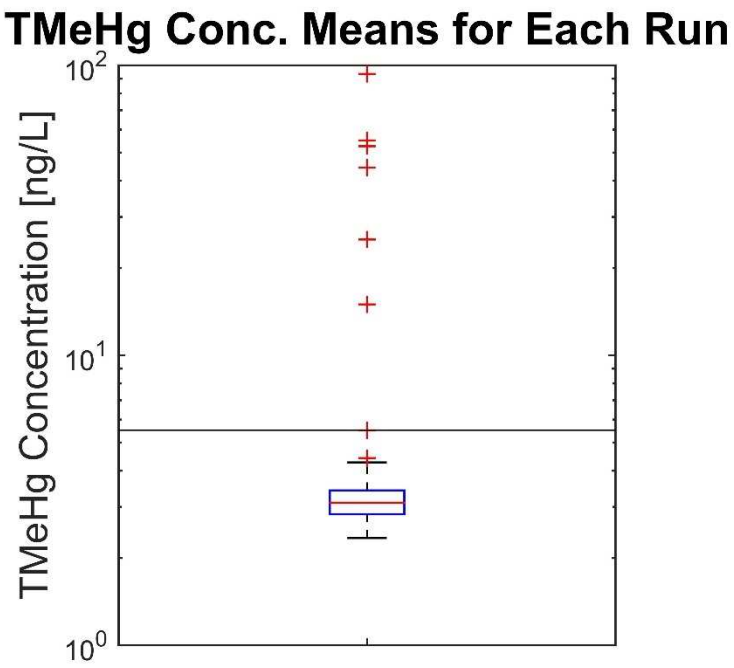

Figure 17: Boxplot of TMeHg mean concentrations from each of the 112 runs for day 165 of the first decade (2000-2009). The red line is the median, the blue lines are the 25th and 75th percentiles, and the black line that crosses the plot is the location of the mean.

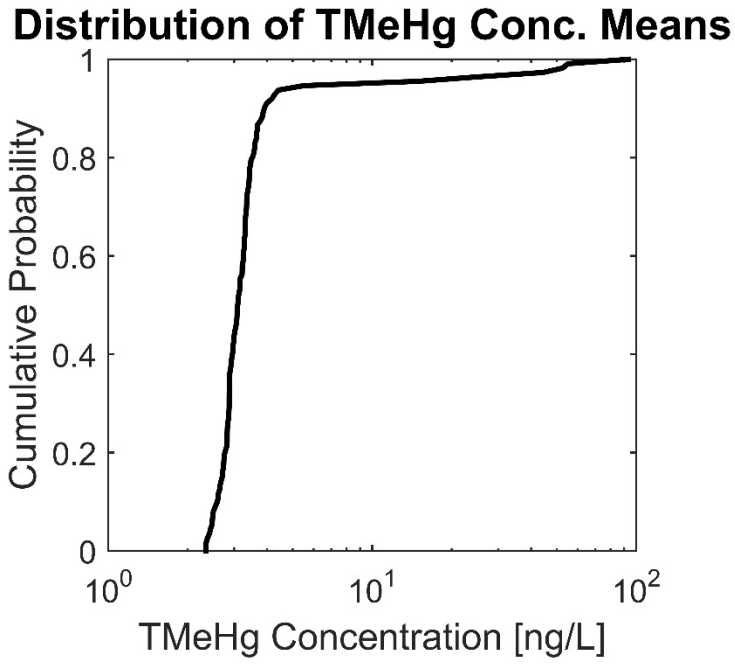

Figure 18: ECDF of the TMeHg mean concentrations for each of the 112 runs for day 165 of the first decade (2000-2009)

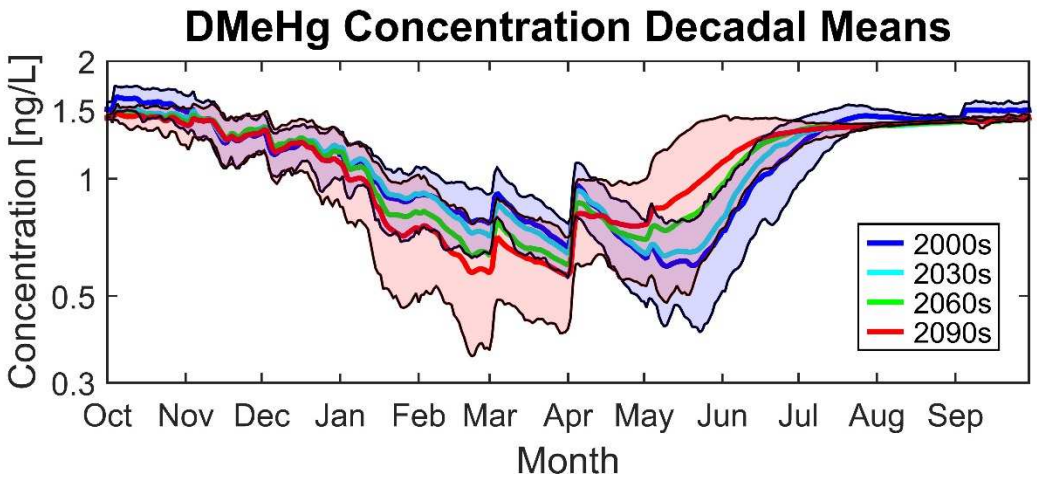

Figure 19: Decadal means of dissolved methylmercury at Weeks Bridge. The first and last decade are enveloped by the 10th and 90th percentiles.

The Hg loading rates were also analyzed for the Weeks Bridge location in order to gain a better understanding of the total amount of Hg passing at this location and what this means for transport of Hg through the river system and into the reservoir. The decadal means for loading rates of THg show similar results to the concentrations, but the difference between the first and last decade in the late spring and summer is less pronounced for loading rates (Figure 20).

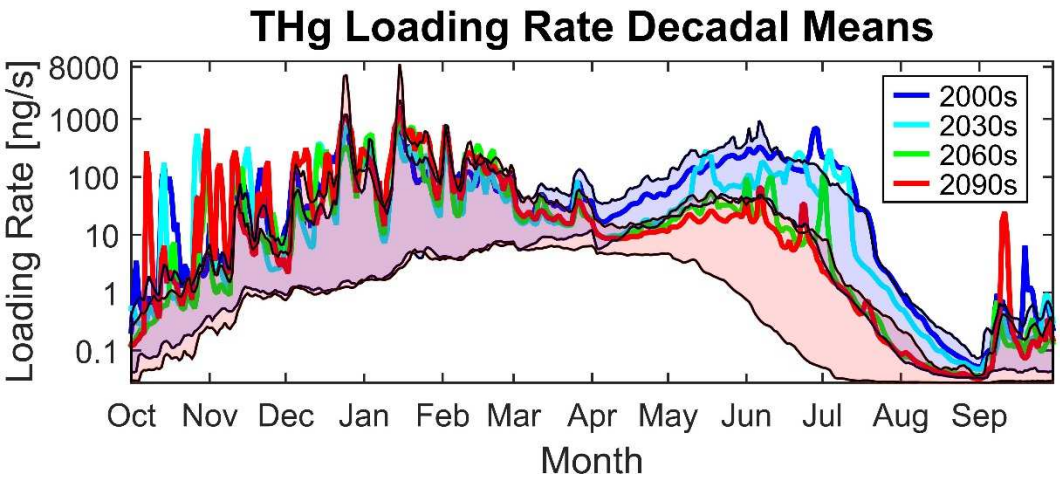

Figure 20: Decadal means of the loads of total inorganic Hg at Weeks Bridge, with the first and last decade enveloped by the 10th and 90th percentiles.

Even though the concentrations for DHg in the last decade are much higher than the concentrations in the first decade during the summer, the loading rates do not show an increase (Figure 21).

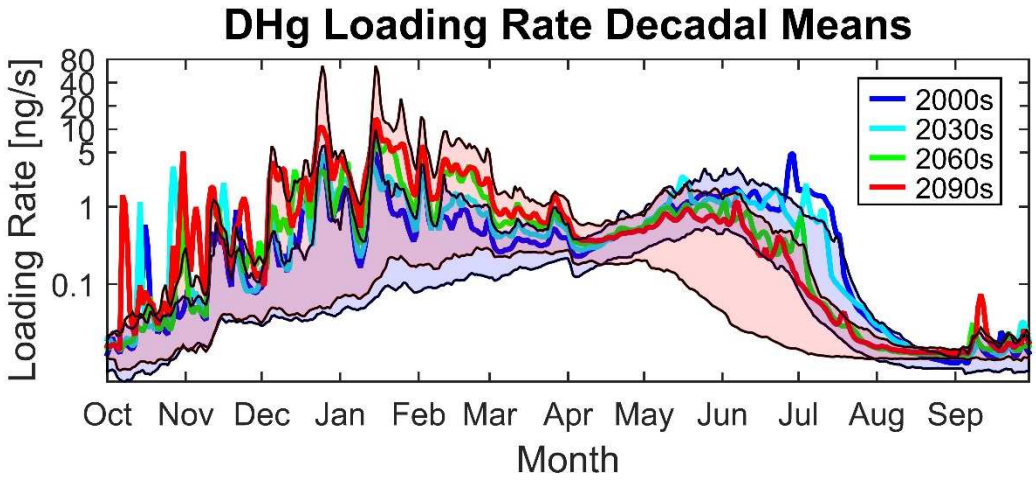

Figure 21: Decadal means of the loads of dissolved inorganic Hg at Weeks Bridge, with the first and last decade enveloped by the 10th and 90th percentiles.

The loading rates decadal means for TMeHg reflect the temporal variations of the concentrations, but there is an increase in noise in the winter for the loading rates (Figure 22).

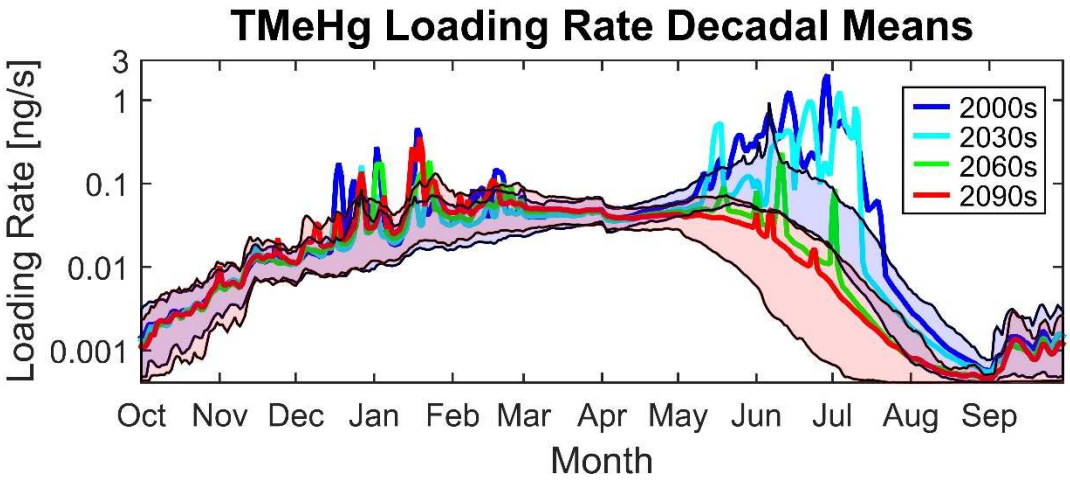

Figure 22: Decadal means of the loads of total methylmercury at Weeks Bridge, with the first and last decade enveloped by the 10th and 90th percentiles.

The decadal means for loading rates of DMeHg (Figure 23) show the lowest values occurring in August through November. This is opposite of the trend seen in the decadal means for concentration (Figure 19) where the lowest concentrations occur in January through May.

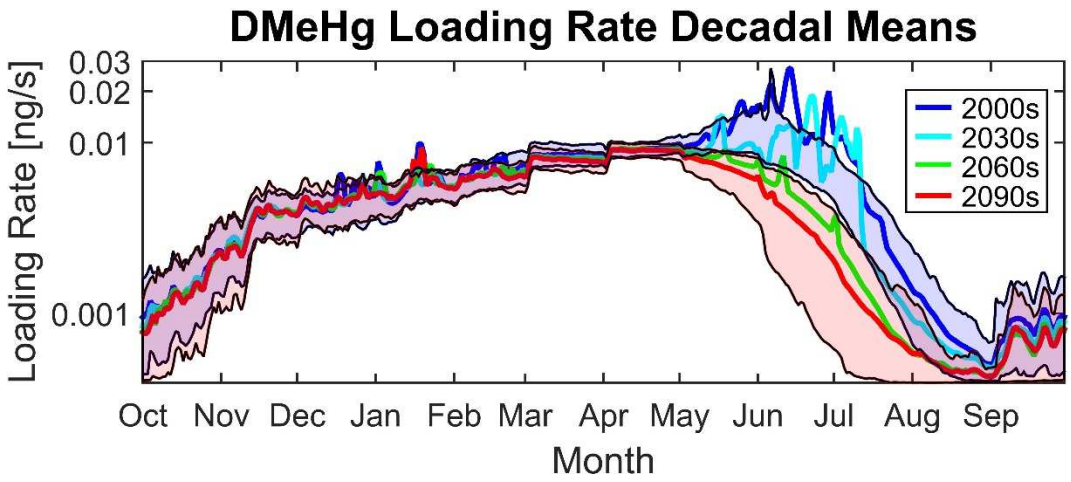

Figure 23: Decadal means of the loads of dissolved methylmercury at Weeks Bridge, with the first and last decade enveloped by the 10th and 90th percentiles.

The two sample KS test results for loading rates show whether each decade has a significantly different distribution compared to the baseline decade (2000-2009) for the Weeks Bridge location. The spring and summer were found to have significant decreases for THg loading rates (Figure 24). Significant increases were found for the fall and winter in some decades, but the majority of the decades had no significant change in these seasons.

Most decades in the winter and spring show a significant increase in DHg loading rates, but the summer shows a significant decrease in most decades and the fall shows no significant change (Figure 25).

All of the seasons see either a significant decrease or no significant change for TMeHg, with the spring and summer experiencing the most significant decrease (Figure 26).

The results for DMeHg (Figure 27) are very similar to the results for TMeHg, with no significant change and significant decrease throughout the board, but with the majority of spring and summer seeing significant decrease.

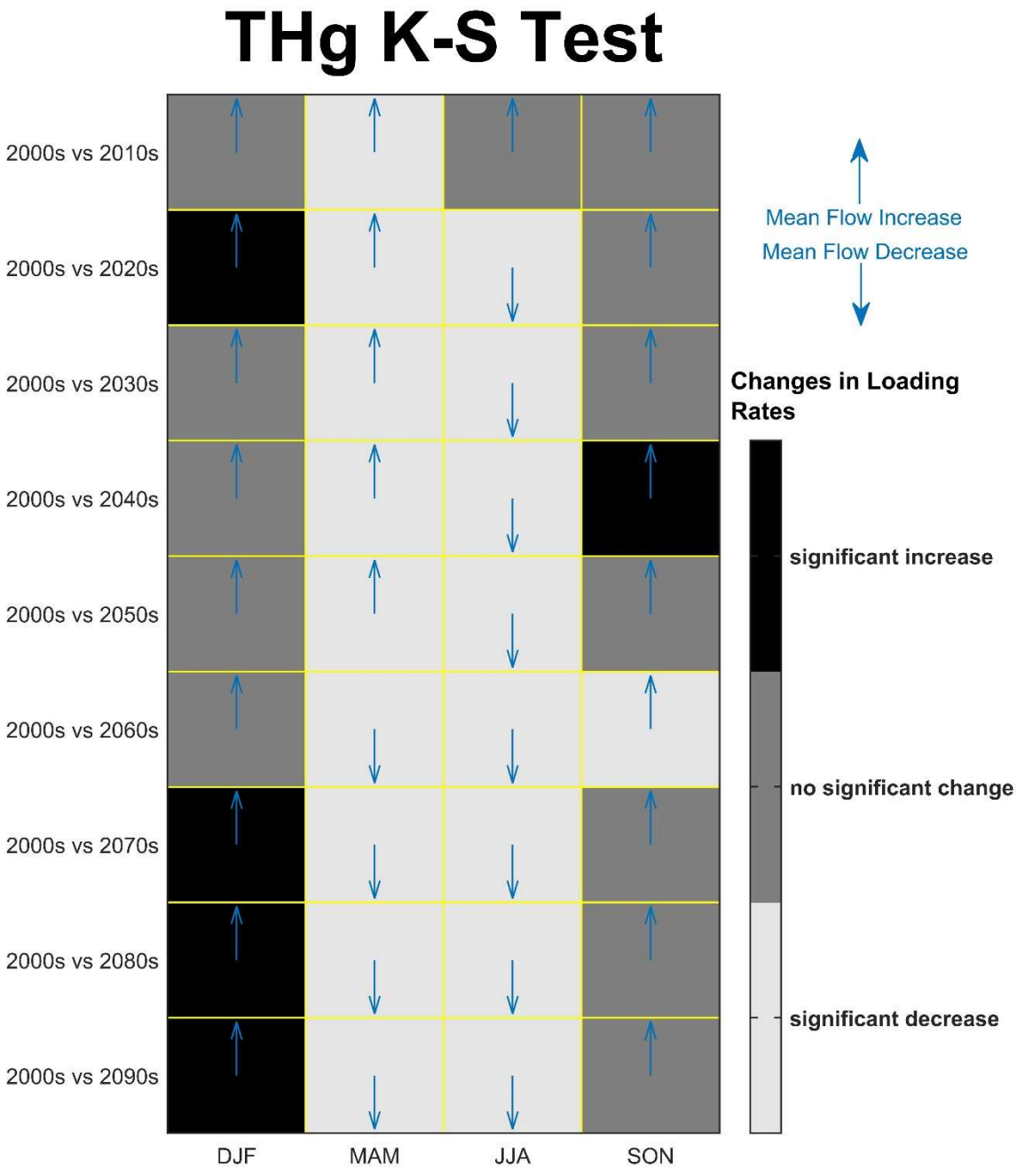

Figure 24: Results of the two sample KS test for total inorganic Hg loads at Weeks Bridge, showing whether each decade has significantly changed compared to the baseline

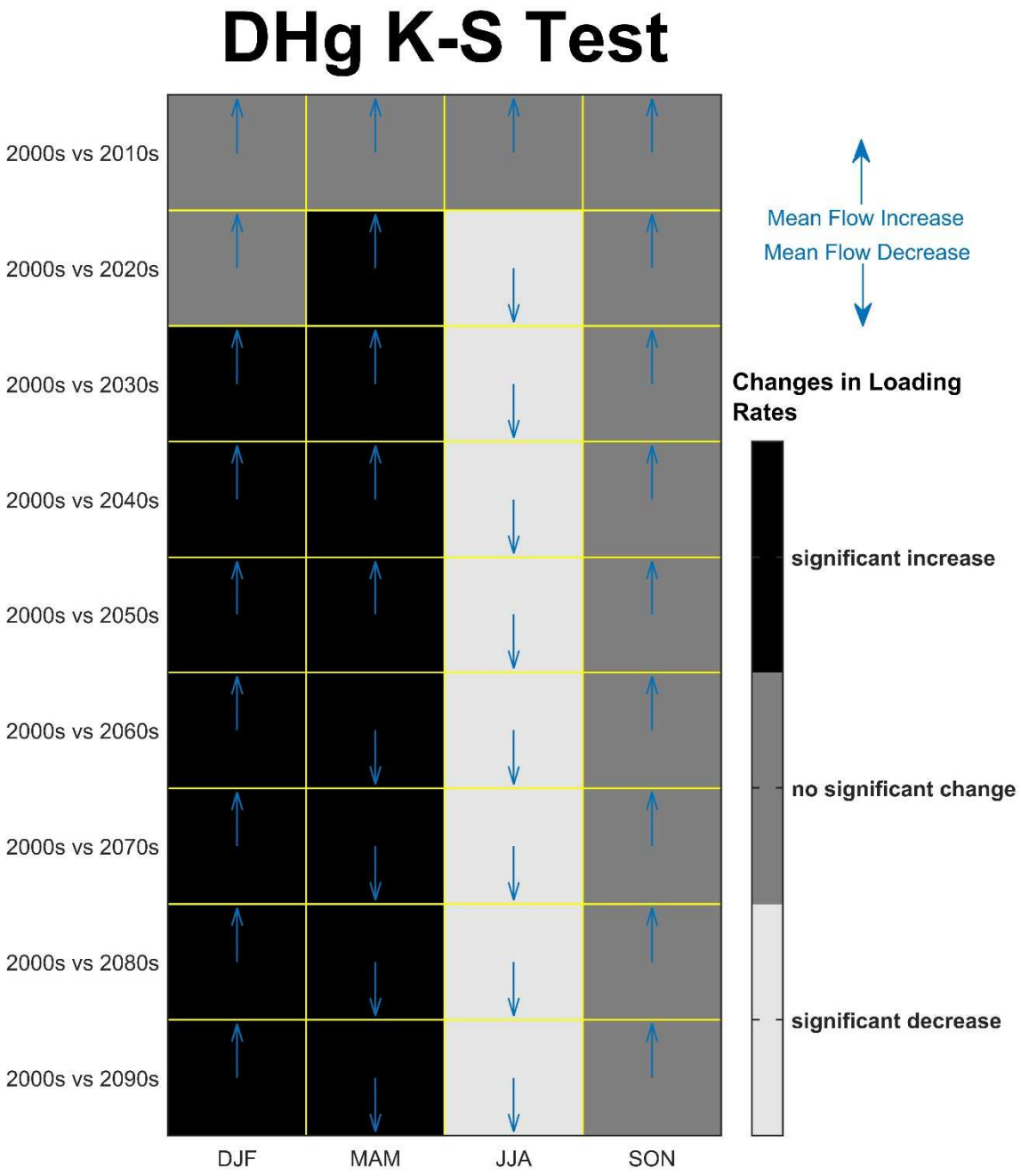

Figure 25: Results of the two sample KS test for dissolved inorganic Hg loads at Weeks Bridge, showing whether each decade has significantly changed compared to the baseline

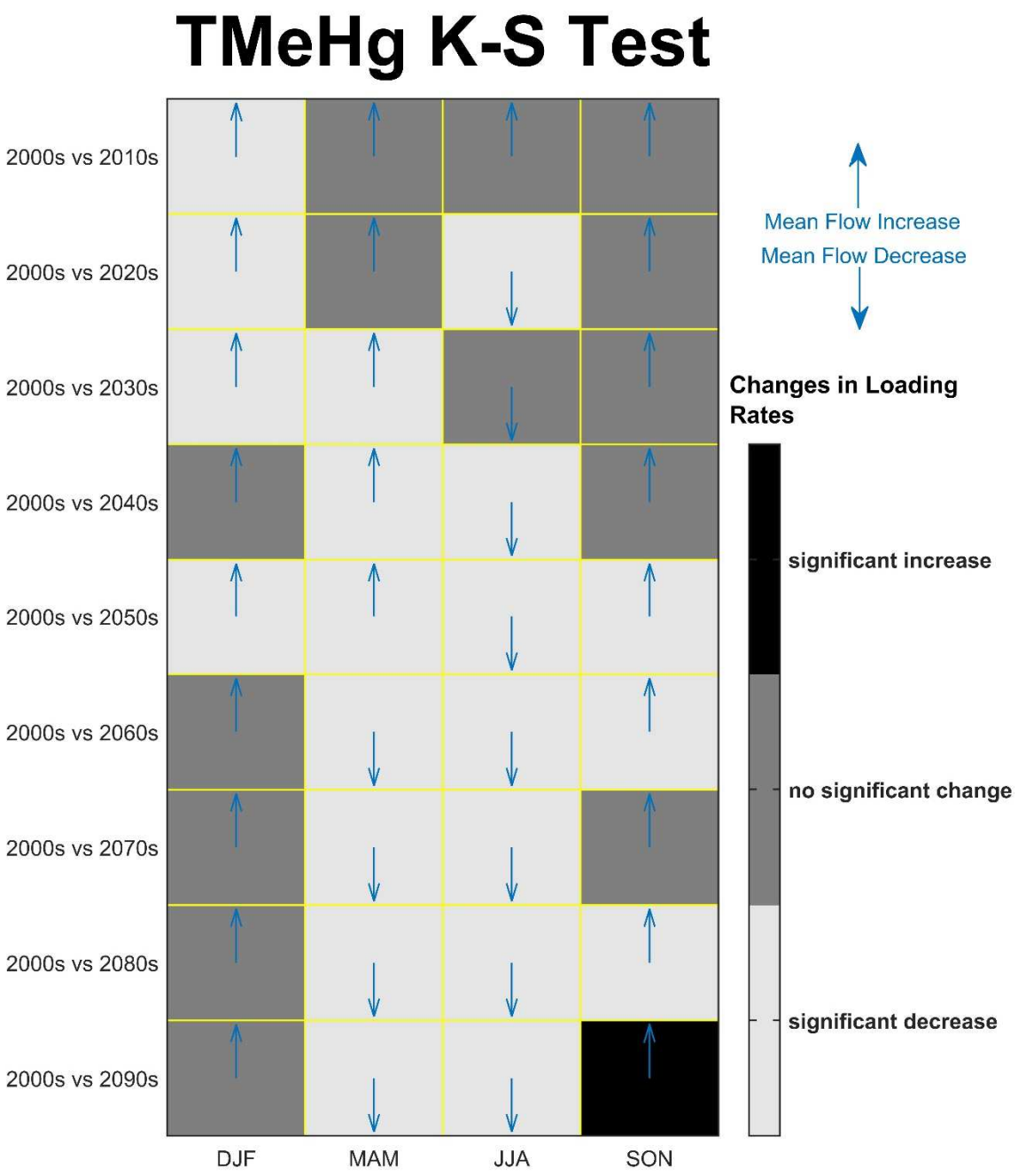

Figure 26: Results of the two sample KS test for total methylmercury loads at Weeks Bridge, showing whether each decade has significantly changed compared to the baseline

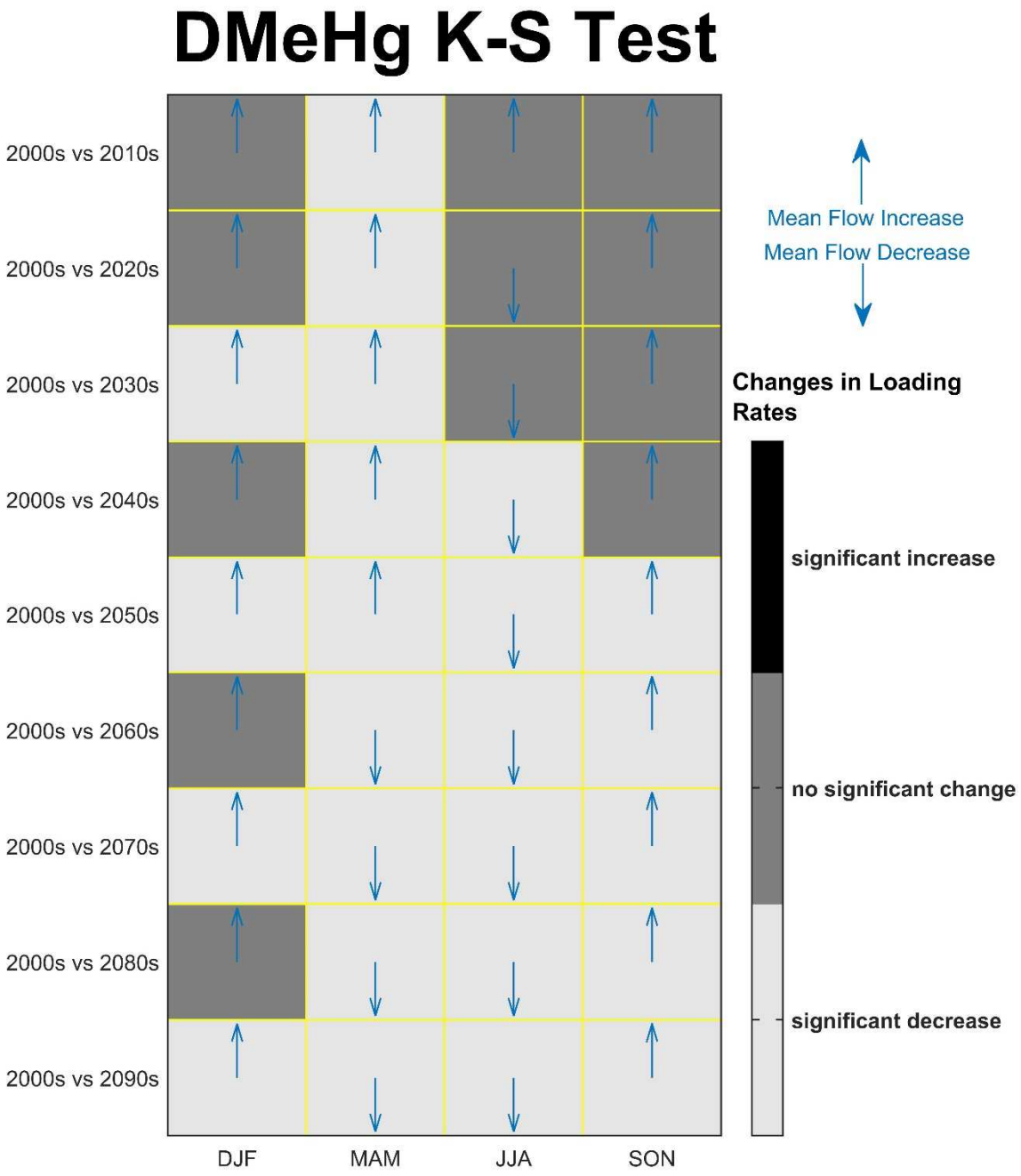

Figure 27: Results of the two sample KS test for dissolved methylmercury loads at Weeks Bridge, showing whether each decade has significantly changed compared to the baseline.

The percent of dissolved Hg and MeHg was also analyzed. There is an increase in percentage of dissolved Hg throughout the year by the end of the century (Figure 28), and a higher percentage of dissolved MeHg in April through July by the end of the century (Figure 29).

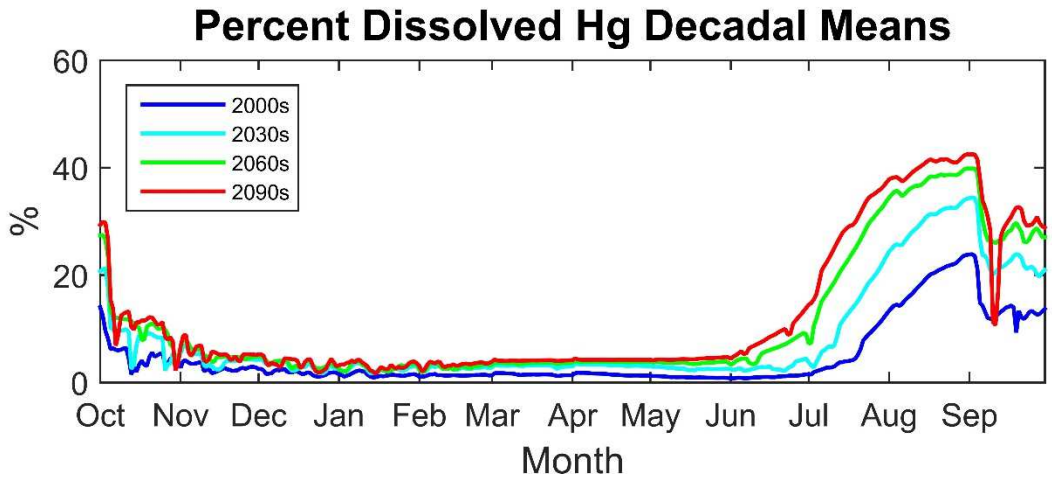

Figure 28: Decadal means for percent of THg that is dissolved at the Weeks Bridge site.

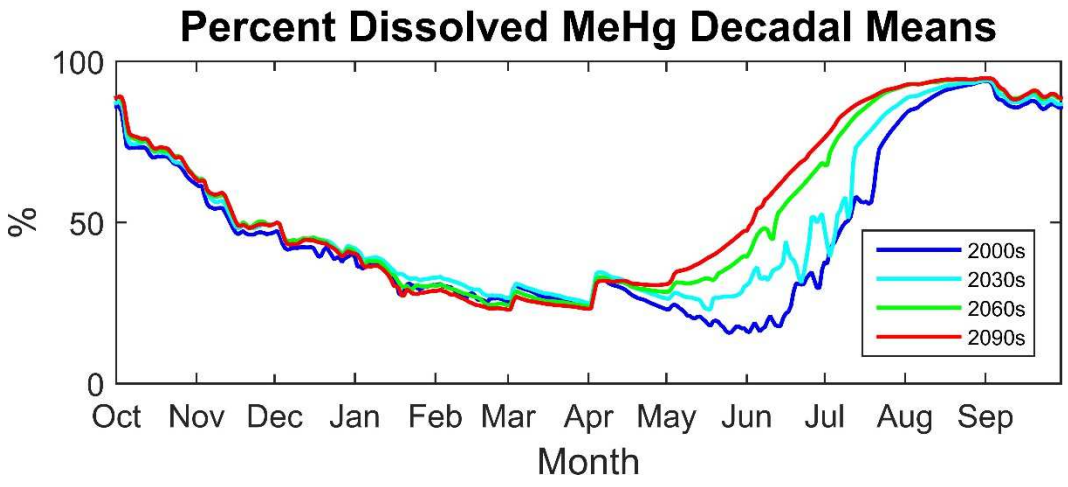

Figure 29: Decadal means for percent of TMeHg that is dissolved at the Weeks Bridge site.

In addition to the Weeks Bridge location, each basin of the reservoir was analyzed for concentrations of DMeHg because of its role in Hg bioaccumulation in fish. A segment was chosen for the approximate center of the South, Middle, and North Basins (model segment 230, 250, and 290, respectively). The results for the South and Middle Basin (Figure 30 and Figure 31) show similar concentrations of DMeHg from January through July, but the South Basin has slightly elevated concentrations of DMeHg during the rest of the year compared to the Middle Basin.

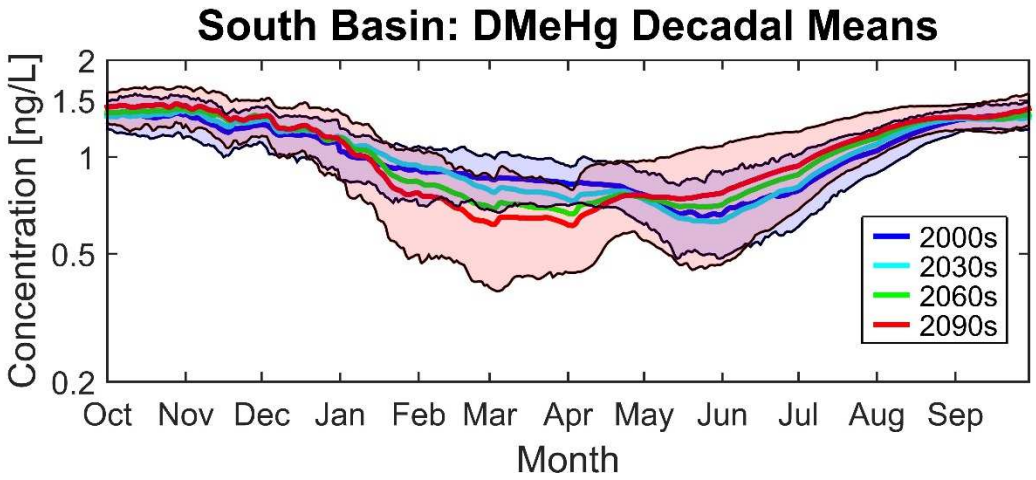

Figure 30: Decadal means of dissolved methylmercury in the Southern Basin, with the first and last decade enveloped by the 10th and 90th percentiles.

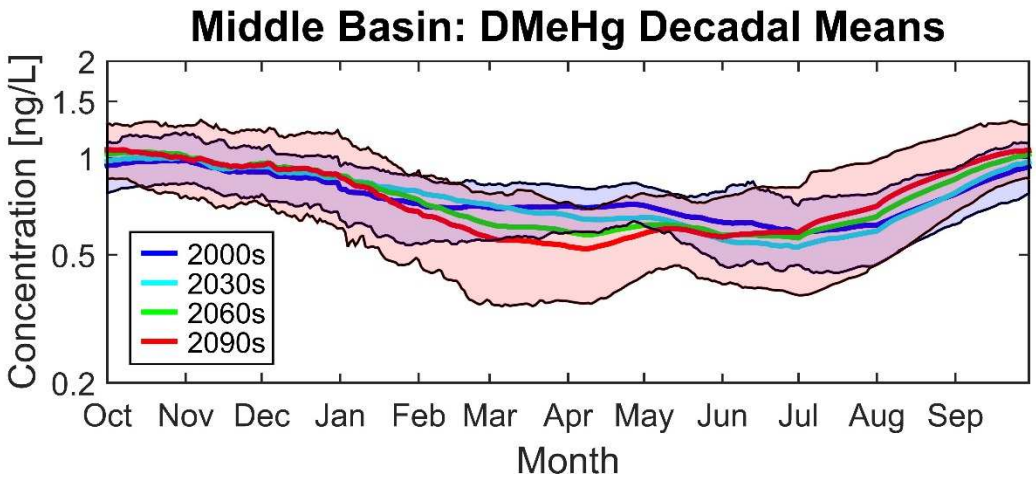

Figure 31: Decadal means of dissolved methylmercury in the Middle Basin, with the first and last decade enveloped by the 10th and 90th percentiles.

The North Basin shows lower levels of DMeHg throughout the year (Figure 32), with the mean concentrations at approximately half the concentration of the first two basins. The temporal variation is also different, as the DMeHg is higher during the late spring and summer compared to the rest of the year while the opposite is true in the first two basins.

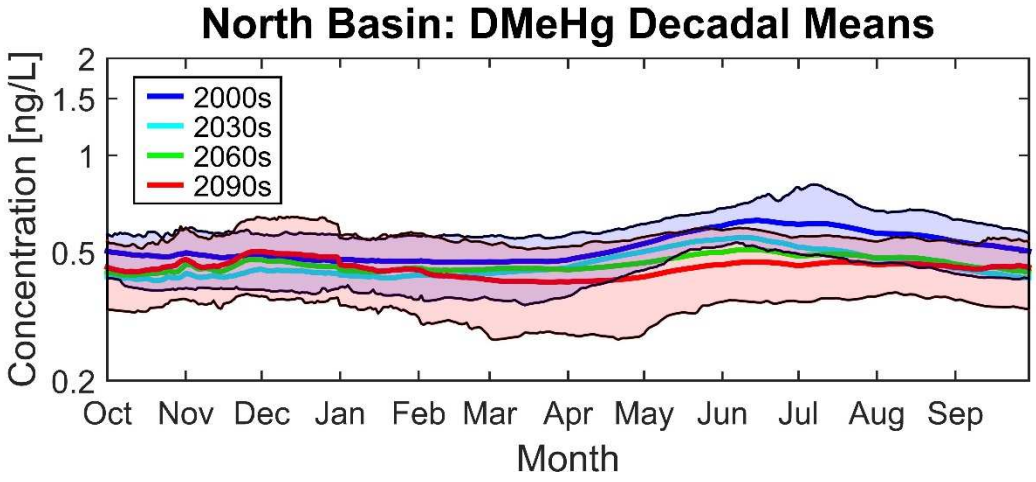

Figure 32: Decadal means of dissolved methylmercury in the Northern Basin, with the first and last decade enveloped by the 10th and 90th percentiles.

Discussion:

The projected changes in flows and channel geometry modify Hg transport and behavior in the Carson River. The decrease of depth over time (Figure 12) is caused by channel widening from bank erosion (Figure 13). These geomorphic changes follow the natural channel evolution that has occurred since the reduction in sediment load, following the decrease in mining, caused the river to downcut through the previously aggraded sediments (Miller et al., 1998). High flow events are a large part of the channel widening process, with the 1997 flood causing an average channel width increase of 30 m (Miller et al., 1999). The high flow events projected to occur in the beginning of the century may contribute large amounts of Hg into the system, but as these high flow events cause the channel to become wider, the magnitude of flow depth and associated bank erosion will potentially decrease by the end of the century.

The decrease in erosion leads to a decrease in THg and TMeHg concentrations and loading rates (Figure 14, Figure 16, Figure 20, and Figure 22). This significant decrease occurs in the spring and summer, which also reflects the decrease in mean flow seen in mid-April through August (Figure 13) and the large decrease in high flows in the summer (Table 1), as the input of Hg in the high flow regime is mainly due to bank erosion.

The timing of DHg variation remains unchanged throughout the century, but concentrations increase noticeably during the summer/fall low-flow period due to a larger stream bottom area (from channel widening) that results in higher bottom diffusive flux (Figure 15 and Figure 21). The decrease in flows during the summer and fall cause the

DHg loads to decrease during these seasons despite the increase in concentration. The results for the two sample KS test that analyze loads reflect this, as significant increases occur in winter and spring with significant decreases occurring in summer, when low flows increase dramatically in frequency.

Similar to DHg, the load decadal means for DMeHg (Figure 23) tell a very different story from the concentrations (Figure 19). Because the highest flows occur during the time when the lowest concentrations of DMeHg occur and the lowest flows occur during most of the time when the higher concentrations of DMeHg occur, the temporal trends of the loads and the concentrations look very different from each other.

The results for DMeHg and TMeHg loading rates are similar (Figure 23 and Figure 27) with the majority of spring and summer seeing significant decrease, and these also reflect the results for THg (Figure 24). This supports the assumption that the decrease in erosion that causes the decrease in THg and TMeHg is also leading to the decrease in DMeHg. The increase in percent of DMeHg (from TMeHg) is also of interest as this shows the percent of TMeHg that is bioavailable. The increase in percent DMeHg in April through July could have negative effects on the bioaccumulation rates of the fish in the river (Figure 29).

Past studies have shown that the Hg levels in the reservoir are strongly dictated by the loading of Hg from the river (Carroll et al., 2010), but the physical differences between the three sections of the reservoir are also an important factor in Hg levels. DMeHg concentration in the South and Middle Basin of the reservoir is lower in winter and higher in late summer/fall by the end of the century. This reflects the shift in timing of

DMeHg loading in the river and temporal changes in inflow to the reservoir. The DMeHg concentrations in the North Basin of the reservoir peak earlier in the year compared to the other basins due to the different residence times in the basins and the transport delay. The basins behave differently as well: the South Basin acts as a river in low flows, the Middle Basin functions more like a reservoir, and the North Basin, while functioning as a reservoir, is diluted by inflow from the Truckee Canal. The Truckee Canal has lower Hg levels than the Carson River, as represented in the model with a constant Hg^{2+} concentration of 25 ng/L and a MeHg concentration of 0.42 ng/L. The decrease in DMeHg concentrations in the North Basin could, therefore, be due to a combination of Hg settling out and dilution from the Truckee Canal.

Limitations:

Similar to all modeled results, the limitation of the Hg transport model need to be considered when analyzing the results. The model is most likely underpredicting the erosion by the end of the century because the model does not have a limit as to how wide a channel can become. The model also does not account for channel avulsion, which is when a channel will migrate during a high flow event to form a new channel. The model instead assumes that the river remains in the original channel and the channel width widens. Because of this, the model is most likely underpredicting the levels of THg, TMeHg, and DMeHg by the end of the century.

The Hg transport model also assumes that the river flow will be equally spread out over the entire channel width. Low flows in channels will usually form inter meandering channels within the main channel. By not accounting for this, the model will over

estimate channel bottom area and underestimate water depth. The overestimation of the channel bottom area in low flows leads to overestimation of DMeHg.

Future Work:

The projected change in frequency of extreme events and the potential effects on the Hg inputs to the system should be further studied. It has been found that the massive amounts of Hg enter the system originate from high flow events, such as the 1997 flood, and the effects of these extreme events were seen in the graphs of decadal means where the mean exceeded the 90^{th} percentile due to outliers. Even though the extreme events are noticeable in these graphs, taking decadal means smooths out the spikes in Hg levels that occur as a result of these events. Using a more appropriate form of analysis to specifically look at the effects of these events would allow for a better understanding of the potential changes in the system.

The effect of the changing temperatures on the transport and speciation of the Hg could also be further studied. The temperature projections could be obtained from the CMIP3 archives, the air temperature changes could be related to stream temperature changes, and the WASP input file could be modified to reflect these stream temperature projections. These stream temperature differences could potentially affect the M/D ratios.

Conclusions:

As the climate is expected to change in Nevada, the effects of hydrologic changes on the transport of Hg in the CRLR should be considered. USBR VIC hydrologic projections from 2000-2099 were used as input data for a physically based, fully dynamic Hg

transport model for the CRLR system in order to see how the system could react to climate change. Analysis of the results for the Weeks Bridge location on the Carson River found that loads of THg, TMeHg, and DMeHg are expected to decrease, significantly in the spring and summer. The decreases in THg and TMeHg are a result of decreased bank erosion due to widened river channels and an overall decrease in flows. The decrease in DMeHg loads is a result of the flows decreasing in the summer, which is when the concentrations of DMeHg saw an increase. The decrease in flows was large enough to effectively drown out the increase in DMeHg and show a decrease in load. DHg loads are expected to increase in the fall and winter by the end of the century, as the increased channel bottom area allows for higher rates of diffusion. The three sections of the reservoir differ in the response of their DMeHg concentrations, with a modest increase during the summer and fall in the South and Middle Basin and an overall decrease in the North Basin. This is due to the North Basin receiving inflow from the Truckee Canal, effectively diluting the concentrations of DMeHg. As flows decrease throughout the century, this inflow has a stronger dilution effect on the North Basin.

BIOACCUMULATION AND MERCURY MASS BALANCE MODEL

Methods:

The BioHg model requires a time series of DMeHg as input. In order to simulate the five year life span of the Sacramento blackfish, the DMeHg decadal median was repeated five times, and the data was sampled every other day in order to follow the program's maximum of 1500 data points. The BioHg model was run for each decade's median, 10^{th} percentile, and 90^{th} percentile. Daily values of micrograms MeHg per gram of mass in a single fish were produced. The results from the runs of this model were then averaged by year to reduce the seasonal variability in MeHg/mass of fish in order to estimate values on a population scale rather than the scale that the model operates on, which is for an individual organism.

BioHg Model Results:

The BioHg model was used to simulate MeHg per mass in Sacramento blackfish based on the DMeHg concentrations of the water. The South Basin shows a slight increase in MeHg per mass over the century (Figure 33). The Middle Basin also shows an increase in MeHg over the century (Figure 34).

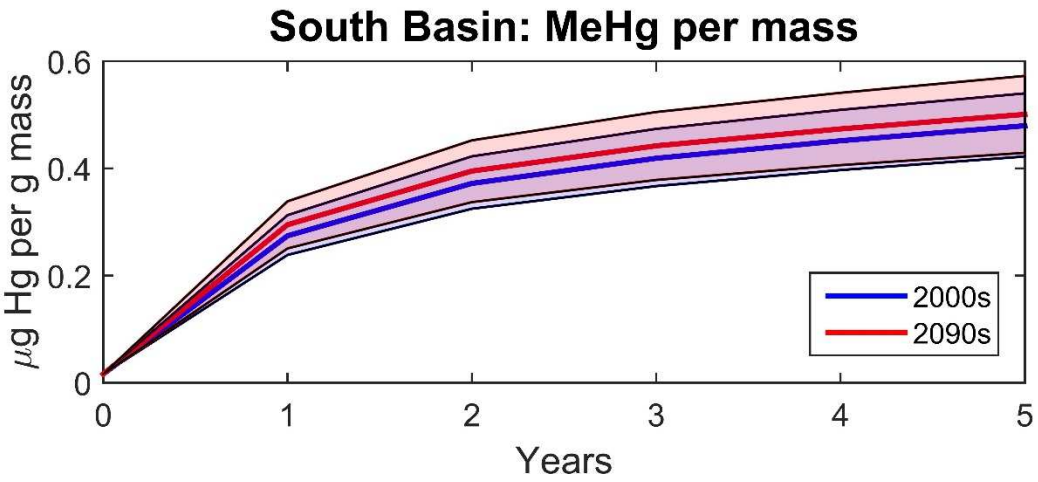

Figure 33: MeHg per mass levels (in µg of Hg per g of fish mass) for the South Basin shown as an annual average over the lifespan of the fish.

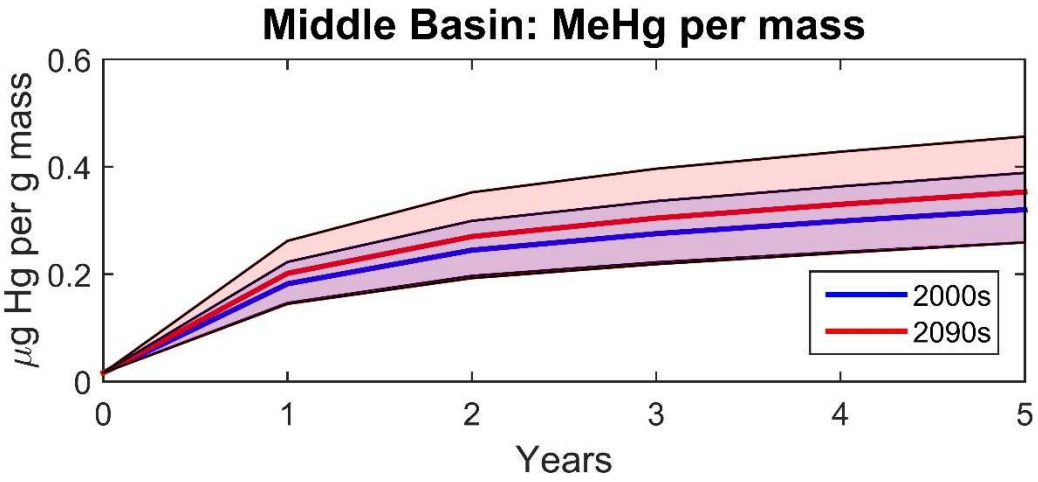

Figure 34: MeHg per mass levels (in µg of Hg per g of fish mass) for the Middle Basin shown as an annual average over the lifespan of the fish.

A decrease in MeHg per mass over the century was found for the North Basin (Figure 35). Overall, the MeHg per mass concentrations are highest in the South Basin and lowest in the North Basin.

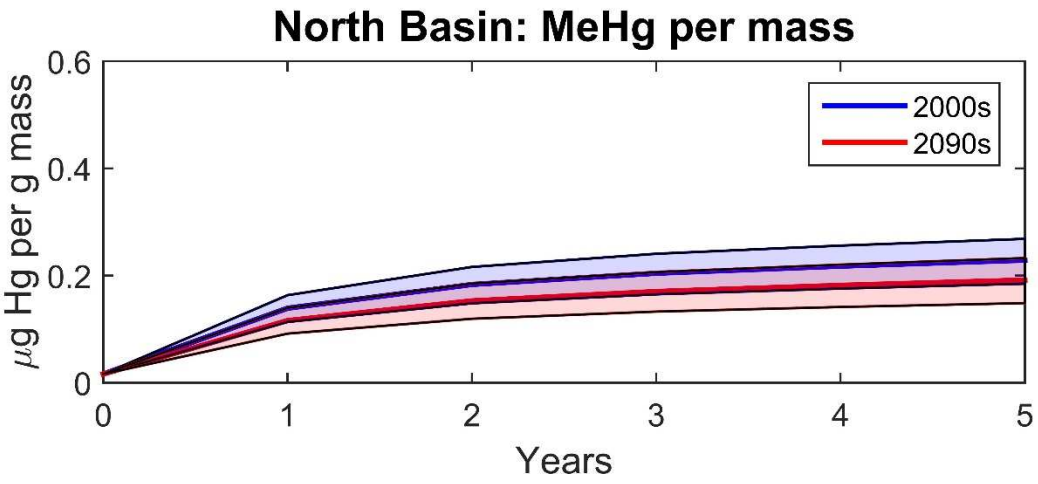

Figure 35: MeHg per mass levels (in µg of Hg per g of fish mass) for the North Basin shown as an annual average over the lifespan of the fish.

Discussion:

The BioHg model results are heavily dependent on the timing of the DMeHg in the reservoirs. The highest consumption rates for the blackfish occur in the warm summer months, and when this peak coincides with high levels of DMeHg in the water, high rates of bioaccumulation occur. The differences in flows between the sections of the reservoirs and the effect that these differences have on the timing of the DMeHg peaks can explain the differences in bioaccumulation between the three sections of the reservoir.

In summer month low flows, the South Basin acts as a river, the Middle Basin acts more like a reservoir, and the North Basin is diluted by inflow from the Truckee Canal. This is reflected by the lower amounts of MeHg per mass in the North Basin compared to the other basins. The contrasting trend of high MeHg per mass in the beginning of the century that occurs in the North Basin is due to the difference in peak DMeHg timing in this reservoir compared to the others as well as the overall decrease in DMeHg

throughout the century. The differences in DMeHg magnitude between the basins of the reservoir is supported by previous sampling efforts where it was found that a significant decrease in Hg occurs from the South Basin to the dam in the North Basin (Bonzongo et al., 1996).

Overall, the results from each of the three scenarios show the fish exceeding the federal consumption advisory level of 1 μg of Hg per g of mass by the end of their first year of life, and this is true for both the first and last decade of the century. These results suggest that the Sacramento blackfish will continue to be unsafe to consume throughout the century unless some sort of mitigation strategy is attempted.

Limitations:

This difference in magnitude of Hg per mass of fish between the three reservoirs could be important for human consumption policies, but the limitations in applying the results of the BioHg model to reality should be considered because the model does not allow for movement of fish between the sections of the reservoir. While the model limits fish to one segment of the reservoir for their water column Hg concentration input, the model was calibrated using samples of fish from multiple sites in the reservoir, so this should reduce the effect that the movement limitation has on the bioaccumulation rate results.

Future Work:

The BioHg model was not altered to take into consideration the increase in water temperature. An increase in temperature would increase the consumption rate of the fish, and this could increase Hg levels in the tissue. Further work could be performed in order

to estimate the increase in water temperature by the end of the century and use this estimation to better simulate the future bioaccumulation rates and tissue Hg levels. The threshold temperature which would cause a significant increase in Hg bioaccumulation rates could also be determined.

Conclusions:

Understanding how the bioaccumulation of Hg in fish in the Lahontan Reservoir will be affected by hydrologic and Hg transport changes in the CRLR system is important for any future investigation of site management. While all three sections of the reservoir show that the fish will exceed federal consumption limits by the end of its first year for both the first and last decade of the century, there is some variation between the sections. The level of Hg per mass by the fifth year for the fish are higher by the end of the century for the South and Middle Basins, while the level is lower at the end of the century for the North Basin due to the timing difference in DMeHg in the reservoir sections and the decrease in DMeHg in the North Basin. Also, the levels of Hg per mass for the fish are higher in the South and lower in the North Basin due to Hg settling out as it travels through the reservoir and the Truckee Canal diluting the North Basin.

REFERENCES

Ambrose, R., Wool, T., Martin, J., Schanz, R., 1991. WASP5. X: A Hydrodynamic and Water Quality Model: Model Theory, User's Manual and Programmer's Guide. USEPA, Athens, Georgia.

Bale AE. 2000. Modeling aquatic mercury fate in Clear Lake, Calif. Journal of Environmental Engineering-ASCE 126(2):153-163.

Bonzongo JC, Heim KJ, Warwick JJ, Lyons WB. 1996. Mercury levels in surface waters of the Carson River Lahontan Reservoir system, Nevada: Influence of historic mining activities. Environmental Pollution 92(2):193-201.

Boudou A, Ribeyre F. 1997. Mercury in the food web: Accumulation and transfer mechanisms. Metal Ions in Biological Systems, Vol 34: Mercury and Its Effects on Environment and Biology 34:289-319.

Carroll, R.W.H., Memmott, J., Warwick, J.J., Fritsen, C.H., Bonzongo, J.C.J., Acharya, K., 2011. Seasonal Variation of Mercury Associated with Different Phytoplankton Size Fractions in Lahontan Reservoir, Nevada. Water Air and Soil Pollution 217, 221-232.

Carroll, R.W.H., Warwick, J.J., 2001. Uncertainty analysis of the Carson River mercury transport model. Ecological Modelling 137, 211-224.

Carroll, R.W.H., Warwick, J.J., Heim, K.J., Bonzongo, J.C., Miller, J.R., Lyons, W.B., 2000. Simulation of mercury transport and fate in the Carson River, Nevada. Ecological Modelling 125, 255-278.

Carroll, R.W.H., Warwick, J.J., James, A.I., Miller, J.R., 2004. Modeling erosion and overbank deposition during extreme flood conditions on the Carson River, Nevada. Journal of Hydrology 297, 1-21.

Collins, M., R. Knutti, J. Arblaster, J.-L. Dufresne, T. Fichefet, P. Friedlingstein, X. Gao, W.J. Gutowski, T. Johns, G. Krinner, M. Shongwe, C. Tebaldi, A.J. Weaver and M. Wehner. 2013. Long-term Climate Change: Projections, Commitments and Irreversibility. In: Climate Change 2013: The Physical Science Basis. Contribution of Working Group I to the Fifth Assessment Report of the Intergovernmental Panel on Climate Change [Stocker, T.F., D. Qin, G.-K. Plattner, M. Tignor, S.K. Allen, J. Boschung, A. Nauels, Y. Xia, V. Bex and P.M. Midgley (eds.)]. Cambridge University Press, Cambridge, United Kingdom and New York, NY, USA.

Cooper, J.J., R.O. Thomas, and Reed, M.S. 1985. Total mercury in sediment, water and fishes in the Carson River drainage, west-central Nevada. Nevada Division of Environmental Protection, Carson City, Nevada.

Cooper, J.J., S. Vigg, R.W. Bryce and Jacobson, R.L. 1983. Limnology of Lahontan Reservoir, Nevada: 1980-1981. Bioresources and Water Resources Centers. Desert Research Institute. DRI Publication 50021.

CIER. 2008. Economic Impacts of Climate Change in Nevada. The Center of Integrative Environmental Research, University of Maryland.

Ecology and Environment, Inc (E&E). 1998. Ecological Risk Assessment Carson River Mercury Site. Prepared for the United States Environmental Protection Agency. ARCS Region 9 and 10. Contract No. 68-W9-0020, Work Assignment No. 20-11-9LR6, Document Control No. ZS3490.

Fontaine TD. 1984. A non-equilibrium approach to modeling metal speciation in acid, aquatic systems – theory and process equations. Ecological Modelling 21(4):287-313.

Gandhi N, Bhavsar SP, Diamond ML, Kuwabara JS. 2007. Development of a mercury speciation, fate, and biotic uptake (biotranspec) model: Application to lahontan reservoir (Nevada, USA). Environmental Toxicology and Chemistry 26(11):2260-2273.

Gangopadhyay, S., Pruitt, T. 2011. West-wide climate risk assessments: bias corrected and spatially downscaled surface water projections. Bureau of Reclamation Technical Memorandum No. 86-68210-2011-01. U.S. Department of the Interior, Bureau of Reclamation, Denver, Colorado.

Golden HE, Knightes CD, Conrads PA, Feaster TD, Davis GM, Benedict ST, Bradley PM. 2013. Climate change and watershed mercury export: A multiple projection and model analysis. Environmental Toxicology and Chemistry 32(9):2165-2174.

Heim, K.J., Warwick, J.J., 1997. Simulating sediment transport in the Carson River and Lahontan Reservoir, Nevada, USA. Journal of the American Water Resources Association 33, 177-191.

Hoffman, R.J., Taylor, R.L., 1998. Mercury and suspended sediment, Carson River Basin, Nevada: loads to and from Lahontan Reservoir in flood year 1997 and deposition in reservoir prior to 1983. US Geological Survey.

Hosseinipour, E., Martin, J., 1990. RIVMOD: A one dimensional hydrodynamic sediment transport model: Model theory and user's guide. USEPA, Athens, Georgia.

Leopold K, Foulkes M, Worsfold P. 2010. Methods for the determination and speciation of mercury in natural waters-A review. Analytica Chimica Acta 663(2):127-138.

Liang X, Lettenmaier DP, Wood EF, Burges SJ. 1994. A simple hydrologically based model of land-surface water and energy fluxes for general-circulation models. Journal of Geophysical Research-Atmospheres 99(D7):14415-14428.

Lindqvist O, Rodhe H. 1985. Atmospheric mercury – A review. Tellus Series B-Chemical and Physical Meteorology 37(3):136-159.

Martin, J., 1992. MERC4: A mercury transport and kinetics model: model theory and user's guide. US EPA, Athens, Georgia.

Maurer EP, Hidalgo HG, Das T, Dettinger MD, Cayan DR. 2010. The utility of daily large-scale climate data in the assessment of climate change impacts on daily streamflow in California. Hydrology and Earth System Sciences 14(6):1125-1138.

McCutcheon SC, Martin JL, Barnwell Jr TO, Maidment D. 1992. Water quality. Handbook of hydrology:11.1-11.73.

Meehl GA, Covey C, Delworth T, Latif M, McAvaney B, Mitchell JFB, Stouffer RJ, Taylor KE. 2007. The WCRP CMIP3 multimodel dataset - A new era in climate change research. Bulletin of the American Meteorological Society 88(9):1383.

Mergler D, Anderson HA, Chan LHM, Mahaffey KR, Murray M, Sakamoto M, Stern AH., 2007. Methylmercury exposure and health effects in humans: A worldwide concern. Ambio 36(1):3-11.

Miller J, Barr R, Grow D, Lechler P, Richardson D, Waltman K, Warwick J. 1999. Effects of the 1997 flood on the transport and storage of sediment and mercury within the Carson River valley, west-central Nevada. Journal of Geology 107(3):313-327.

Miller, J.R., Lechler, P.J., Desilets, M., 1998. The role of geomorphic processes in the transport and fate of mercury in the Carson River basin, west-central Nevada. Environmental Geology 33, 249-262.

Miller WP, Piechota TC, Gangopadhyay S, Pruitt T. 2011. Development of streamflow projections under changing climate conditions over Colorado River basin headwaters. Hydrology and Earth System Sciences 15(7):2145-2164.

Miskimmin BM, Rudd JWM, Kelly CA. 1992. Influence of dissolved organic-carbon, pH, and microbial respiration rates on mercury methylation and demethylation in lake water. Canadian Journal of Fisheries and Aquatic Sciences 49(1):17-22.

Morel FMM, Kraepiel AML, Amyot M. 1998. The chemical cycle and bioaccumulation of mercury. Annual Review of Ecology and Systematics 29:543-566.

Petrie B, Yeats P. 1990. Simple models of the circulation, dissolved metals, suspended solids, and nutrients in Halifax Harbor. Water Pollution Research Journal of Canada 25(3):325-350.

Risley J, Moradkhani H, Hay L, Markstrom S. 2011. Statistical Comparisons of Watershed-Scale Response to Climate Change in Selected Basins across the United States. Earth Interactions 15:26.

Schiedek D, Sundelin B, Readman JW, Macdonald RW. 2007. Interactions between climate change and contaminants. Marine Pollution Bulletin 54(12):1845-1856.

Smith, G.H., with new material by Joseph Tingley. The History of the Comstock Lode, 1850-1997.

Somlyody, L. 1978. An effort for modelling the transport of micropollutants in rivers. Proceedings of: Modelling the Water Quality of the Hydrological Cycle, IAHS Press, Inst. of Hydrology, Wallingsford, Oxfordshire, England, 39–49.

Trudel, M., Rasmussen, J.B., 2001. Predicting mercury concentration in fish using mass balance models. Ecological Applications, 11(2): 517-529.

Wang QR, Kim D, Dionysiou DD, Sorial GA, Timberlake D. 2004. Sources and remediation for mercury contamination in aquatic systems - a literature review. Environmental Pollution 131(2):323-336.

Warwick, J.J., Carroll, R.W., 2010. Evaluating the impacts of uncertainty in geomorphic channel-changes on predicting mercury transport and fate in the Carson River system, Nevada. Proceedings of the Annual International Conference on Soils, Sediments, Water and Energy, p. 21.

Warwick, J.J., Heim, K.J., 1995. Hydrodynamic modeling of the Carson River and Lahontan Reservoir, Nevada. Water Resources Bulletin 31, 67-77.

Whitehead, P.G., Wilby, R.L., Battarbee, R.W., Kernan, M., Wade, A.J., 2009. A review of the potential impacts of climate change on surface water quality. Hydrological Sciences Journal-Journal Des Sciences Hydrologiques, 54(1): 101-123.

Wiener JG, Evers DC, Gay DA, Morrison HA, Williams KA. 2012. Mercury contamination in the Laurentian Great Lakes region: Introduction and overview. Environmental Pollution 161:243-251.